Robotic Human Enabled Intelligent Aerial Analysis

A Venus mission proposal with modular aerial vehicles for detailed scientific data collection.

Submitted by:

Frank Huynh
Basil Russell-McCorkle
Banglue Wei
Christopher McCullough
Carolina Ramos Ocasio

Avik Banerjee
Samina Patel
Nyla Duhon
Oliver Thornhill
Adil Shirinov

Faculty advisor:

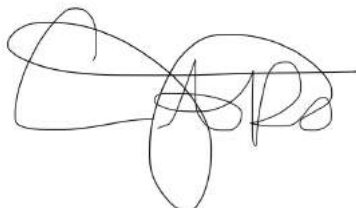Dr. Álvaro Romero-Calvo

Basil Russell-McCorkle #1584967

Samina Patel #1602063

Frank Huynh #1602911

Carolina Ramos Ocasio #1603402

Avik Banerjee #1255117

Adil Shirinov #1179546

Nyla Duhon #1603324

Oliver Thornhill #1603218
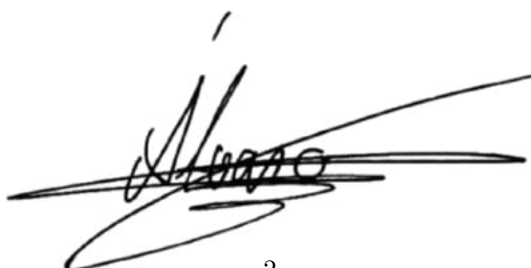
Christopher McCullough #1146458

Banglue Wei #1252713

Faculty Advisor:
Dr. Álvaro Romero-Calvo #978289

2

Contents

4

1 Executive Summary

RHEIA^2 is an proposed mission to explore our twin planet – Venus. The mission responds to a request for proposal (RFP) from the American Institute of Aeronautics and Astronautics to design a human-enabled robotic mission to Venus. Per the RFP, RHEIA^2 is designed to leverage astronauts in orbit around Venus to maximize science return and address long unanswered questions about Venus's atmosphere and surface. The period of direct human involvement and science return is designed to last no longer than 30 days.

The primary driver of the RHEIA^2 mission design is to properly justify bringing astronauts to Venus to help facilitate science return. After thoroughly investigating controllability, the team deemed this to be an inadequate justification for the costs associated with bringing humans to another planet. With current advances in machine learning algorithms and autonomous vehicles [1], it is extremely likely that a vehicle on Venus could have this capability in a decade's time and that this would be meaningful even within the relatively short mission timescales imposed by the harsh surface conditions. Additionally, even with advances in high temperature electronics [2], the lifetime of a surface vehicle system as a whole would be extremely short, making the prospect of a singular vehicle insufficient for exploration. Distributed networks and modular vehicles solve this problem: the early conclusion of a single vehicle's mission does not significantly decrease science return if there are multiple vehicles to collect science. This, however, highlights another issue: volume constraints in the launch vehicle. Multiple vehicles are required for a distributed network and, fully assembled, are going to be difficult to pack inside of a payload fairing along with the necessary supporting architecture. RHEIA^2 proposes a solution to these issues: by leveraging in-space manufacturing, disassembled science vehicles can be sent to the astronauts. Saving on volume, this allows for large number of vehicles to be sent to Venus that the astronauts will then assemble in Venus orbit prior to deployment.

RHEIA^2's unique mission architecture consists of four primary vehicles: the Interplanetary Transfer Module (ITM), the low altitude balloons referred to as Chariots, the static drops, and the Deep Space Transport, sometimes referred to as the Interplanetary Transfer Vehicle (ITV) for generality. The Deep Space Transport is NASA's only publicly available architecture to support human interplanetary exploration, so RHEIA^2 will consider this to be the human vehicle for this mission. Because it is the human vehicle, it is outside of the scope of this report, but some discussion of the Deep Space Transport is necessary to describe the RHEIA^2 mission architecture.

The ITM is a crucial element in RHEIA^2's mission architecture. The module, designed to be a forefront mission element for human assembly and manufacturing, contains an organized and efficient workspace for the Venus crew to assemble RHEIA^2's science payloads. During the initial stage of the mission, the

ITM launches via SpaceX's Falcon Heavy into low Earth orbit (LEO) carrying the science payloads and necessary subsystems to sustain the module during its two-day transfer to dock with the ITV. During the module's LEO transit, an ADCS configuration consisting of an Inertial Measurement Unit (IMU), Inertial Navigation System (INS), star trackers, and horizon sensor pairs with the ITM's four ASCENT-helium propulsion modules to maneuver the ITM. A patch antenna on the ITM provides communications between the module and NASA's Deep Space Network (DSN) during LEO transit to facilitate tracking and maneuvering efforts. For docking with the ITV, a VHF antenna establishes communications between the ITM and the ITV once the ITM is within a 1 km range of the ITV. The communications architecture pairs with MIL-STD-1773 online data handling (ODH) bus for efficient data processing. To power the active subsystems aboard the ITM, four lithium thionyl chloride batteries are used, with enough energy to sustain the module's subsystem demands for at least three days. The ITM's Aluminum 2024 structure is designed to withstand the launch loads the module will experience with SpaceX's Falcon Heavy; additionally, a meteorite and debris protection shield (MDPS) with Aluminum 2024 and Kevlar layers mitigates impact and radiation risks in the LEO, Venus transit, and Venus orbit environments.

To further protect the ITM in the LEO environment, the module possesses a passive thermal control architecture with a double-aluminized Kapton MLI blanket and an exterior 0.0001 mils black annodized aluminum thermal coating to regulate the module's interior temperature around 20°C. Once docked with the ITV through the module's passive docking adapter, the ITM begins to draw power, thermal regulation, and ECLSS resources from the ITV for the rest of the mission duration. The ECLSS aboard the ITM features a fan assembly for regulating airflow in the module, four HP 2book 15 laptops for astronaut use, two fire extinguishers, and a Luxfer S106W air tank to combat helium gas leaks in the module. Within the

Figure 1: Complete ITM design.

astronaut workspace on the ITM, footholds, strap hooks, and compartment racks enable an effective and organized work environment for the astronauts to assemble the RHEIA[2] science payloads. For payload deployment, the astronauts use a linear actuator system similar to heritage payload deployment configurations to deposit the science payloads into the Venusian atmosphere through the ITM's integrated airlock. Ultimately, the Interplanetary Transfer Module is designed based on heritage International Space Station (ISS) modules as a modification to NASA's Deep Space Transport. Moreover, the ITM presents an exciting opportunity for reusable applications in human-involved scientific exploration, assembly, and manufacturing for future manned planetary missions.
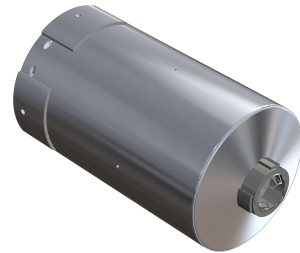
The Static Drops are the secondary scientific vehicle of the RHEIA[2] mission. The probe architecture

serves two main objectives: collecting preliminary data/science and targeting science objectives that could not be done with the Chariot architecture. In this case, the static drops will contain a large suite of instruments focusing on atmospheric characterization of Venus' upper to lower atmosphere.

RHEIA^2's static drop architecture is inspired by current proposed Venus missions such as NASA's DAVINCI and Rocket Lab's Morning Star. The 55 cm diameter and 60 kg probe consists of 3 main components: RF transparent E-glass back shell, titanium alloy pressure vessel, and ablative carbon phenolic heat shield. Within the pressure vessel contains the instrument suite, communications, and power subsystems.

Similar to the Chariots, the probes start their journey by being deployed from the ITM after being deorbited by SRBs. Once the probes enter the Venusian atmosphere, they start collecting science upon hitting the target altitude during the hour long descent. During this descent data is transmitted to the ITM before the static drop completes its mission by disassembling on contact with the Venusian surface. Unlike the Chariot architecture, the Static drops are manufactured on Earth before being placed within the ITM. It is worth noting the introduction of the static drop architecture allows for the opportunity to create a ride-share program where other agencies or institutions can bid for a spot within the ITM to be deployed.

Figure 2: Proposed Static Drop

Currently the RHEIA^2 has accounted for 3 static drops within the ITM; however, future refinement of the mission may allow for an increased number.

The Chariot is the primary scientific vehicle of the RHEIA^2 mission. Each vehicle is comprised of a scientific instrument module held within a titanium shell made from two halves, sealed by an O-ring. The shell is filled with a mixture of Helium and water vapor, which serve to maintain outward pressure against the high-pressure lower atmosphere. In addition, to propel the vehicle towards Venus, each Chariot is fitted with two solid rocket motors, four reaction wheels, and a Sigratherm heat shield.

To maximize efficient use of the available storage space, the Chariots are stored as stacked components which the crew assembles inside the ITM. The stored components and assembly method are likewise set up to minimize danger to the crew; the shell is assembled using only hand tools and involves no welding or grinding, which would create a fire hazard. The solid rocket motors use Ammonium Nitrate propellant, specifically chosen for its lowered likelihood of producing toxic residue and dust in the ITM.

A Chariot's mission begins when the ITM's linear actuator throws one out of the airlock. From here, the Chariot will drift away from the ITM for approximately 5.56 minutes to gain a safe distance of 10 meters

and fire the entry boosters. While the Chariot is drifting, the reaction wheels will work to keep the boosters pointing retrograde before they fire. The boosters will fire for approximately 5 seconds, inducing a ΔV of 300 m/s retrograde.

The Chariot enters the atmosphere Heat Shield-first, and reaches the lower atmosphere in approximately 33 minutes. As it approaches 28 kilometers above the surface, it releases 10% of its internal gas to alleviate outwards pressure. The Chariot's altitude will stabilize at 5 kilometers above the surface, where it takes in 0.034 kilograms of CO_2 to maintain a survivable inwards pressure differential.

The Chariot conducts studies at 5 kilometers above the Venusian surface for approximately 4.1 to 4.2 days, relying on a combination of high-temperature electronics and phase change materials to maintain an operational temperature. A patch antenna will transmit any scientific data gained as the ITM passes overhead. With current predicted developments of system technology, thermal control is predicted to fail first, and thus is the chief limiting factor of the Chariot's lifespan.

Figure 3: Chariot with boosters, heat shield, and reaction wheels.

RHEIA[2] plans for the ITM to be launched to low Earth orbit (LEO) in early 2033. The ITM will be fully packed with the module science vehicle components, and rendezvous with the NASA Deep Space Transport. The Deep Space Transport will then begin its transfer to Venus taking roughly 4 months. One the DST has completed the Venus insertion maneuver, the 30 day science mission will begin. The static drops will be released first via the ITM's linear actuator and will deorbit using a pair of solid rocket boosters. Following this, the chariots will be assembled one at a time inside the ITM and the be deployed with the same method as the static drop. Following the end of the 30 day science mission, the DST will depart from Venus and begin its journey to bring the astronauts back to Earth.

From research and development to mission closeout, RHEIA[2] is projected to cost 996.4M. This includes contingency, and is within the maximum budget provided by the RFP. This mission establishes clear and compelling justification for bringing astronauts to Venus – utilizing in space manufacturing and pioneering the first mission of its kind. The in space manufacturing approach will allow for greater science return, and the science gained from successful deployment of the static drops and chariots will be instrumental in developing our knowledge of Venus's history, atmosphere, and geology. Beyond the mission itself, the ITM is a versatile piece of equipment that could be used for similar deployment in LEO, Lunar orbit and beyond.

2 Mission Overview

2.1 Mission Objectives

Table 1: RHEIA^2 Mission Objectives

ID	Requirement
RHEIA^2-1	The RHEIA^2 science mission shall last no longer than 30 days in orbit around Venus
RHEIA^2-2	The RHEIA^2 mission shall cost no more than \$1B USD in the fiscal year 2023.
RHEIA^2-3	The RHEIA^2 mission shall launch no later than December 31st, 2037, and the science mission shall conclude no later than December 31st, 2039.
RHEIA^2-4	The RHEIA^2 mission shall perform distributed science collection in the low Venusian atmosphere.
RHEIA^2-5	The RHEIA^2 mission shall provide insight to previously unknown atmospheric chemistry.
RHEIA^2-6	The RHEIA^2 mission shall determine the presence of volcanic activity at the Venusian surface.
RHEIA^2-7	The RHEIA^2 mission shall pioneer a new class of in-space manufacturing missions.

2.2 Science Missions

The Venus Exploration Analysis Group (VExAG)[1] is NASA's community-based forum designed to provide scientific input and technology development plans for planning and prioritizing the exploration of Venus over the next several decades. Open to all interested scientists, VEXAG regularly evaluates Venus exploration goals, scientific objectives, investigations, and critical measurement requirements, including recommendations in the NRC Decadal Survey and the Solar System Exploration Strategic Roadmap.

RHEIA^2's science objectives are derived directly from VExAG and for the demonstrative purposes of this proposal only a few key focuses were selected. The criterion for selecting the objectives for the mission were: 1) Diversity of Science, 2) Difficulty of Obtaining Data, 3) Possible Cost of Obtaining Data. An advantage of RHEIA^2 is the modular nature of the mission. Adding and removing science objectives can be as simple as swapping out a payload package. Table 2 shows all the VEXAG objectives and those selected for our mission.

---

[1] https://www.lpi.usra.edu/vexag/.Consulted on 05/01/2024

Table 2: RHEIA² Science Objectives Highlighted

Goals	Objectives	Investigations	GOI Code
Atmosphere	Atmospheric Evolution	Solar Nebula/noble gases	I.A.1
		Atmospheric Escape	I.A.2
	Radiative balance, climate, and superrotation	**Global circulation**	**I.B.1**
		Radiative Balance	**I.B.2**
		Vertical motions	I.B.3
	Clouds and Haze characterization	**Cloud chemistry**	**I.C.1**
		Greenhouse/ Cloud physics	**I.C.2**
		Role of lightning	I.C.3
		Biologically relevant chemistry	**I.C.4**
Surface and Interior	**Geodynamics**	Stratigraphy/deformation	II.A.1
		Radiogenic He4 Ar40 in atmosphere	**II.A.2**
		Geophysical studies	**II.A.3**
		Active volcanism and tectonism	**II.A.4**
		Absolute rock ages	II.A.5
	Differentiation	Elemental composition	II.B.1
		Large scale composition variations	II.B.2
		Structure of crust	II.B.3
		Core and mantle structure	II.B.4
		Radiogenic crustal elements	II.B.5
		Subsurface layering	II.B.6
Interior Surface and Atmosphere	Liquid water and the greenhouse effect	History of water from Isotopes	III.A.1
		Role of water in Tessera	III.A.2
		Hydrous minerals and sediments	III.A.3
	Interactions of interior-surface and atmosphere over time	Elemental composition-noble gas	III.B.1
		Rock weathering investigations	**III.B.2**
		Altitude profiles of reactive species	**III.B.3**
		Sulfur outgassing from surface	III.B.4

2.3 Concept of Operations

Concept of Operations
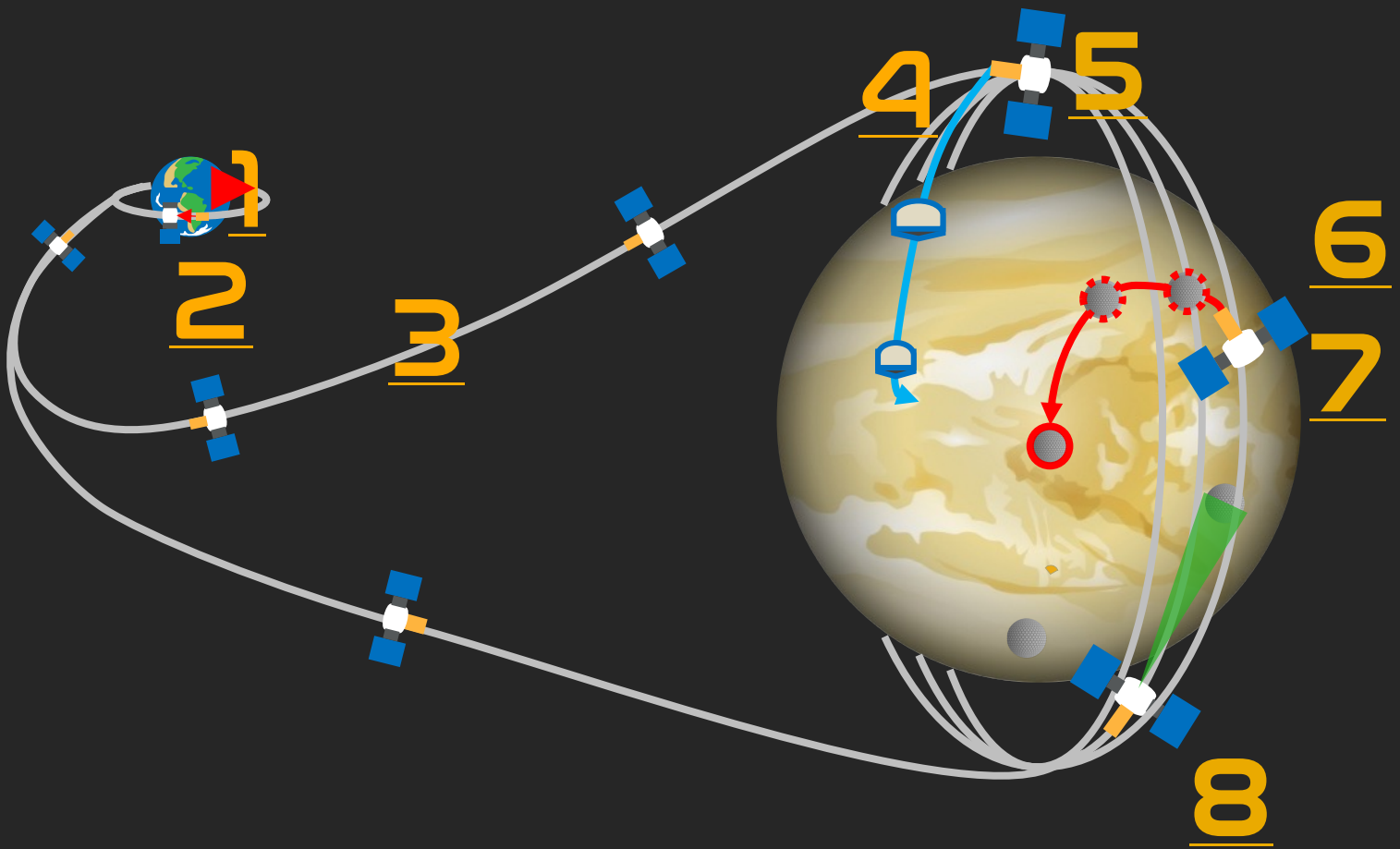
3   Vehicle Trade Study Overview

The team determined early on that the most scientific gains would be made by re-approaching a mission into Venus' lower atmosphere, possibly ground level. The precedent for such a mission is Venera 13 in 1982, which landed on the surface of Venus and survived 127 minutes[3]. The team reasoned that modern technologies such as high temperature electronics would allow a new mission to revisit this environment, survive significantly longer, and gain more science in the process.

Low cost and crew assistance are key pillars of the mission. As such, a chosen vehicle must be relatively simple, survivable, and able to offer extra capabilities thanks to the crew in orbit.

Ultimately, the most prominent architecture base came from Geoffrey Landis' "Low Altitude Exploration of Venus by Balloon," which discussed both a design for a medium-altitude balloon functioning at 21 km and designs for a low-altitude balloon hovering at 5 km, where the pressure is 698 K, the pressure is 6.7 MPa, and the density is 50 kg/m^3[4]. The latter design was free-drifting without any control mechanisms and relied on a titanium shell to withstand the pressure differential at 5 km. As an added advantage, the balloon's specialization in low altitudes meant it could be denser and thus more compact to store. the group proceeded in studies with this design, resulting in the Chariot.

4   Mission Trajectory Analysis

The overarching mission trajectory incorporates detailed analyses conducted at each crucial mission phase. This includes the precise rendezvous and docking maneuvers of the interplanetary transfer module (ITM) with NASA's deep space transport (DST) while in low-Earth orbit (LEO). Following this initial docking phase, the mission trajectory includes the transfer from LEO to low Venus Orbit (LVO). During this segment, care was taken to ensure that the transfer was optimized for fuel efficiency and time, minimizing Environmental Control and Life Support Subsystem (ECLSS) requirements and risks associated with interplanetary travel.

Upon reaching LVO, the next critical step involves the strategic deployment of various scientific probes and Chariots designed to explore Venus's atmosphere and surface. This phase involves deploying these instruments to maximize their operational capabilities and scientific return. It should be noted that the payload deployment, while simulated, will realistically be adapted in real-time by astronauts onboard the DST-ITM vehicle. This introduces dynamic capability in our mission allowing astronauts to choose which science instruments to place on the Chariots and where to deploy both the Chariots and probes.

Along with the deployment from orbit, baseline simulations were conducted regarding the entry, descent,

and landing of the Chariots to their designated operational areas on Venus. Similar considerations are made for the probes, but these vehicles will not be deployed to a particular altitude but will rather crash and burn into the surface after collecting and transmitting science data throughout the atmosphere. These simulations were crucial in validating the mission's theoretical and practical feasibility, refining mission details, and confirming that the trajectory aligns with existing technology and objectives.

4.1 Rendezvous and Docking of ITM with DST

One fundamental assumption for this mission is that NASA's Deep Space Transport (DST) will operate in a slightly elliptical 400 km altitude LEO orbit [5]. Our spacecraft, the ITM, will launch aboard a SpaceX Falcon Heavy rocket to a lower, slightly elliptical 250 km altitude orbit to rendezvous and dock with the DST. This operation is divided into two phases: rendezvous and docking. Initially, during the rendezvous, the ITM (chaser) performs a series of orbital maneuvers to match orbits with the passive DST (target), gradually approaching it through precise ground track maneuvers. The docking involves the chaser closing in and attaching to the target. Crucially, the nature of the spacecraft as passive or active must be distinguished from that of their docking ports, which are detailed in Sec. 5. For a successful rendezvous, the orbital planes of both spacecraft must align. This is typically achieved by timing the ITM's launch to ensure it enters the correct orbital plane, avoiding the high delta-v costs associated with plane change maneuvers. Once aligned, the ITM enters a phasing orbit, drawing incrementally closer to the DST with each orbit due to a slight difference in orbital periods. Accurate timing of this orbit insertion allows the spacecraft to converge precisely at their closest approach points after several orbits, thus completing the rendezvous. Since the target and chaser are in the same orbital plane, Lambert's solvers can be used for a large part of the rendezvous and docking with the final rendezvous/docking dynamics (at close range) governed by the Clohessy Wiltshire equations

$$\ddot{x} = 3n^2x + 2n\dot{y}, \tag{1}$$

$$\ddot{y} = -2n\dot{x}, \tag{2}$$

$$\ddot{z} = -n^2z \tag{3}$$

where n is the mean motion of the orbit, x, y, and z are the relative positions in the radial, along-track, and cross-track directions, respectively [6].

A MATLAB simulation using the Optimization toolbox, Simulink, and Aerospace toolbox was designed to carry out these maneuvers and simulate docking similar to that of vehicles docking to the International

Space Station (ISS) [7]. For the simulation, we position the chaser 1 km below the target along the radial position vector with zero relative velocity as it transitions from rendezvous to docking. The docking sequence unfolds in three phases: initial approach, transposition, and final approach [8]. In the initial approach or $\bar{r}$ approach, the chaser progresses toward the target along the radial position vector using translational thrusters at approximately 0.3 m/s, reducing the distance to 100 m [9]. During this phase, it is crucial to maintain the relative velocity component perpendicular to the $\bar{r}$ at zero. As the chaser ascends from below, its orbital angular velocity decreases, requiring compensation through perpendicular thruster firings. If these thrusters fail, the chaser's resultant lag is a safety mechanism, preventing potential collisions by slowing its approach (and phasing it in the opposite direction to the target). During the transposition phase, the chaser reorients to docking attitude and maneuvers around the target to align approximately 20 m in front of the docking port. If a direct path between positions during transposition risks collision due to the target's attitude, the chaser maneuvers such that it offsets by 20 m along the body z-axis, maintaining a zero offset along the body y-axis. This maneuver occurs on the x-z plane of the body frame while in docking attitude. In the final phase, the chaser decreases its speed to 0.03 m/s as it closes the last 10 meters, carefully aligning the docking ports for connection. To model all of these different, complicated maneuvers in the simulation, In the simulation setup, we define initial orbital parameters, attitude control vectors, and key docking metrics such as relative distance and velocities. The rendezvous maneuvers are structured as an optimization challenge to minimize delta-v, adhering to orbital mechanics and timing constraints. We fine-tune maneuver parameters using MATLAB functions like fsolve and fmincon, obtaining optimal timings and ΔV vectors. Our mission simulation leverages a Simulink model, capturing the dynamics, guidance, and control systems of both spacecraft. The chaser's guidance system handles burn commands for rendezvous and docking guidance, while the target maintains a stable attitude. Control systems convert these commands into thruster forces and moments. Simulation results, including spacecraft positions and maneuvers, are dynamically visualized in a satellite scenario viewer, comprehensively displaying the entire process. All of the rendezvous and docking maneuvers and corresponding visualizations are captured in Fig. 4 and all key parameters from the simulation are captured in Table 3. Specifics of propellant required and corresponding values of thrusters will be discussed in Sec. 5.

Table 3: Simulation Parameters for Rendezvous and Docking

Parameter	Value
Total ΔV	169.75 m/s
Total Propellant Required	849.44 kg
Initial Docking Velocity (10+ m)	0.3 m/s
Final Soft Docking Velocity	0.03 m/s
Total Time Required (Rendezvous + Docking)	2.06 days
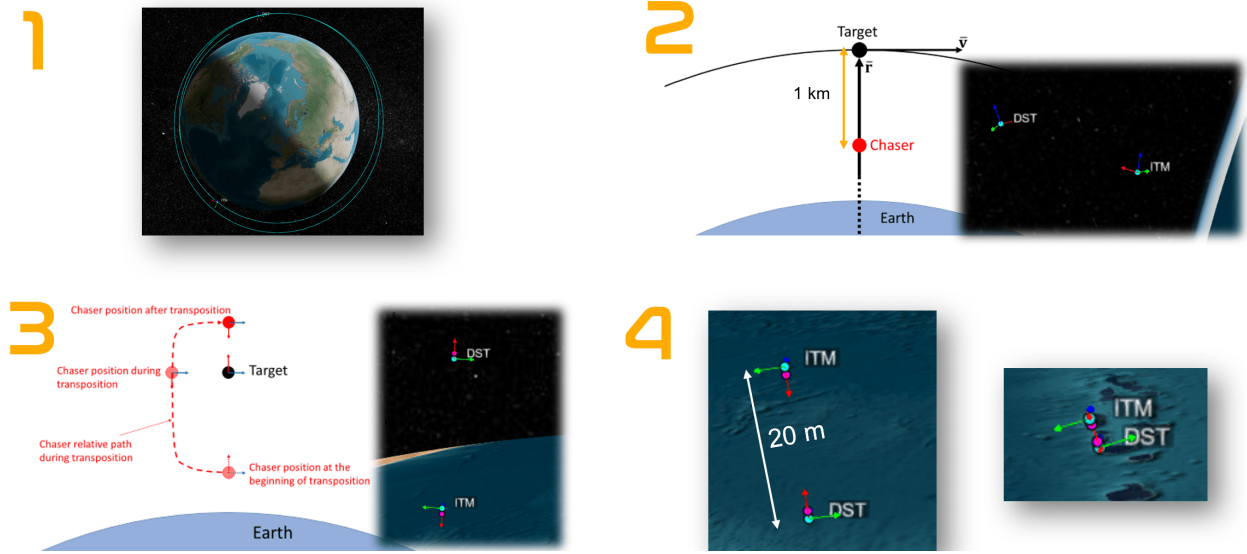
Figure 4: Image of the four-step process for rendezvous and docking. **Step 1** (top left) involves orbit phasing, where the chaser spacecraft maneuvers to align its orbit with that of the target, ensuring both orbits are coplanar and phased correctly. **Step 2** (top right) is the R-bar approach, where the chaser moves within 1 km of the target along the radius vector shown ($\bar{r}$) to maintain a safe and controlled trajectory. **Step 3** (bottom left) covers the transposition maneuver, during which the chaser reorients to a docking attitude and carefully maneuvers around the target to position itself roughly 20 meters in front of the docking port, avoiding any collisions. **Step 4** (bottom right) involves the final approach, as the chaser steadily closes in at 0.3 m/s. Once within 10 meters of the target, it slows down to 0.03 m/s until the docking ports align and the chaser successfully docks with the target.

4.2   Interplanetary Transfer

The interplanetary transfer of the ITM and DST following successful docking is determined based on the AIAA RFP, which states that the mission should launch no later than December 31, 2037, with the crew-operated science mission completed no later than December 31, 2039. A detailed interplanetary trajectory selection process employs the NASA Ames Trajectory Browser, complemented by a custom MATLAB script that uses JPL planetary ephemeris datasets in conjunction with the MICE library—NASA's SPICE toolkit adapted for MATLAB [10, 11]. This dual-faceted approach facilitates the identification of prospective launch windows, pinpointing those that yield optimized trajectories characterized by minimized ΔV requirements. Optimal trajectories found through a combination of these tools are primarily in 2034 or 2037, as shown in Fig. 5.

SPK ID	Name	Abs Mag	Size	Orbit condition code	Earth Departure	Destination Arrival	Destination Departure	Earth Return	Stay time ▾	Duration	Injection C3 (km^2/s^2)	Abs DLA	Injection ΔV (km/s)	Post-Injection ΔV (km/s)	Total ΔV (km/s)	Reentry speed (km/s)	Route
299	Venus		12104 km	0	Nov-12-2037	Feb-05-2038	Feb-25-2038	Nov-12-2038	20 days	365 days	19.4	2°	4.08	2.73	6.81	13.84	EV-VE
299	Venus		12104 km	0	Jun-11-2034	Dec-08-2034	Jan-07-2035	Nov-13-2035	30 days	1.42 yrs	13.7	6°	3.83	1.49	5.32	14.16	EV-VE
299	Venus		12104 km	0	Jun-06-2034	Dec-03-2034	Jan-02-2035	Nov-03-2035	30 days	1.41 yrs	13.4	3°	3.82	1.52	5.34	14.04	EV-VE
299	Venus		12104 km	0	Jun-11-2034	Dec-03-2034	Jan-02-2035	Nov-03-2035	30 days	1.4 yrs	14	7°	3.85	1.53	5.37	14.04	EV-VE
299	Venus		12104 km	0	Jun-11-2034	Dec-03-2034	Jan-02-2035	Oct-29-2035	30 days	1.38 yrs	14	7°	3.85	1.58	5.42	14.01	EV-VE
299	Venus		12104 km	0	Jun-11-2034	Dec-03-2034	Jan-02-2035	Oct-24-2035	30 days	1.37 yrs	14	7°	3.85	1.66	5.51	13.98	EV-VE
299	Venus		12104 km	0	Jun-11-2034	Dec-03-2034	Jan-02-2035	Oct-19-2035	30 days	1.36 yrs	14	7°	3.85	1.78	5.63	13.97	EV-VE
299	Venus		12104 km	0	Aug-10-2034	Dec-03-2034	Jan-02-2035	Nov-08-2035	30 days	1.25 yrs	7.8	23°	3.57	2.08	5.65	14.1	EV-VE
299	Venus		12104 km	0	Aug-10-2034	Dec-03-2034	Jan-02-2035	Nov-03-2035	30 days	1.23 yrs	7.8	23°	3.57	2.09	5.66	14.04	EV-VE
299	Venus		12104 km	0	Aug-15-2034	Dec-03-2034	Jan-02-2035	Nov-03-2035	30 days	1.22 yrs	8.8	23°	3.62	2.07	5.69	14.04	EV-VE
299	Venus		12104 km	0	Nov-02-2037	Feb-15-2038	Mar-17-2038	Jan-16-2039	30 days	1.2 yrs	15	5°	3.89	1.84	5.72	14.27	EV-VE

Figure 5: NASA Ames Trajectory Browser data showing a variety of optimal trajectories between 2034 and 2037 sorted by Earth departure date [10].

From this list of possible trajectories, the final selection was underpinned by prioritizing minimal mission duration (to yield more feasible ECLSS requirements) and a required 30-day orbital stay at Venus. Here, parameters from the AMES trajectory browser were compared with the MATLAB-derived porkchop plots shown in Fig. 6 were generated using the MATLAB script to validate and supplement the parameters obtained using the trajectory tool. Based on this cross-referencing, the trajectory in Fig. 4 was optimized for all the key parameters. The MATLAB script was also used to calculate the additional propellant required onboard the DST to complete the interplanetary trajectory docked with the ITM. This additional propellant required is calculated for two propulsion architectures: (1) assuming the DST uses a hybrid propulsion architecture including both chemical and electric propellant or (2) just chemical propellant [12]. In the hybrid architecture, it is assumed that chemical propulsion is used for the planetary departure burns, and electric propulsion is used for the arrival burns to circularize. These parameters are also shown in Table 4. In the event of a launch abort or unforeseen circumstances, additional backup trajectories in 2034 were also selected and are shown in Table 5 and Table 6.

Figure 6: MICE MATLAB script Porkchop plots of the contours of departure C3 (left) and arrival V'_∞ (right), each providing optimal launch windows for an interplanetary mission by mapping the relationship between the initial departure and arrival dates. The color gradients represent energy requirements: C3 for departure and V_∞ for arrival speed (km/s).

Figure 7: Primary Interplanetary Trajectory Visual

Table 4: Primary Interplanetary Trajectory

Mission Timeline and ΔV	
Date	ΔV
Earth Departure Jun-06-2034 180-day transfer	3.82 km/s (C3 = 13.4 km^2/s^2, DLA = -3°)
Venus Arrival Dec-03-2034 30-day stay	396 m/s
Venus Departure Jan-02-2035 305-day transfer	1.12 km/s
Earth reentry Nov-03-2035 1.41-yr total mission	0 km/s (14.04 km/s reentry speed) **5.34 km/s total ΔV**
Propulsion Requirements	
Hybrid Propulsion (Chemical and Electric)	**Chemical Propulsion (CP)**
Additional DST CP Usage with ITM Docked (kg) 10604.31	Additional DST CP Usage with ITM Docked (kg) 10944.93
Additional DST EP Usage with ITM Docked (kg) 59.26	

Table 5: Backup Interplanetary Trajectory 1

Mission Timeline and ΔV	
Date	ΔV
Earth Departure Jun-11-2034 180-day transfer	3.83 km/s (C3 = 13.7 km^2/s^2, DLA = -6°)
Venus Arrival Dec-08-2034 30-day stay	380 m/s
Venus Departure Jan-07-2035 310-day transfer	1.11 km/s
Earth reentry Nov-13-2035 1.42-yr total mission	0 km/s (14.16 km/s reentry speed) **5.32 km/s total ΔV**

Table 6: Backup Interplanetary Trajectory 2

Mission Timeline and ΔV	
Date	ΔV
Earth Departure Aug-10-2034 115-day transfer	3.57 km/s (C3 = 7.8 km^2/s^2, DLA = 23°)
Venus Arrival Dec-03-2034 30-day stay	969 m/s
Venus Departure Jan-02-2035 310-day transfer	1.11 km/s
Earth reentry Nov-08-2035 1.25-yr total mission	0 km/s (14.04 km/s reentry speed) **5.65 km/s total ΔV**

4.3 Chariot Entry, Descent, and Landing (EDL)
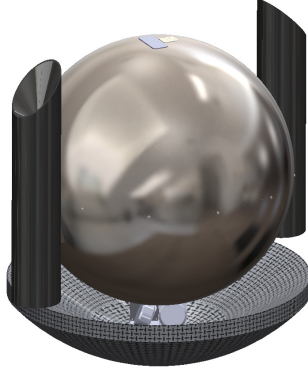
(a) Chariot EDL Configuration.
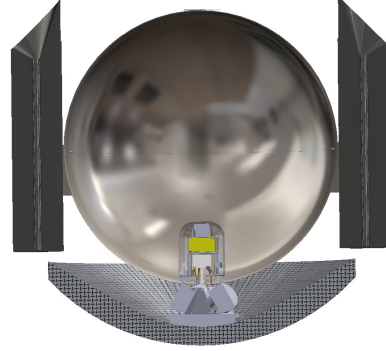
(b) Chariot EDL Cutaway view.

After being assembled by the crew in orbit, the Chariots are launched from the ITM out of the airlock. From there, an array of reaction wheels will keep them pointed retrograde for approximately 5.56 minutes to let them drift 10 meters from the ITM. Afterwards, a pair of solid rocket boosters will activate, decelerating the balloons and putting them on a trajectory for atmospheric entry. Individual subsystems of the EDL system will be described in their own sections below.

Table 7: Chariot EDL requirements.

ID	Requirement
CHAR-EDL-01	The Chariot shall be placed on a suborbital trajectory to enter Venus' atmosphere.
CHAR-EDL-02	The Chariot shall slow down sufficiently to mitigate thermal and heat loads and avoid hitting the ground.
CHAR-EDL-03	The Chariot's density shall allow it to float at 5 km after EDL is complete. a

4.4 Chariot Heat Shield

Aside from internal protection, TCS features an ablative heat shield. The heat shield is constructed from Sigratherm, a carbon phenolic material with proven reliability in high-temperature space applications [13]. Properties of Sigratherm appear in table 9. First-order simulations predict almost all thermal loads on the heat shield will subside by 100 km. The shield is designed to ablate completely at 70 km, but complete ablation will not be completely guaranteed due to intangible aerodynamic inconsistencies. Thus, a pyrotechnic device will decouple the heat shield before the chariot begins operation. Using a sizing script and equation[4], the overall heat shield characteristics can be ascertained in table 10.

$$T_i^n = \frac{-k\triangle t}{\rho c_p \triangle x_i^2} T_{i-1}^{n+1} + (1 + \frac{2k\triangle t}{\rho c_p \triangle x_i^2}) T_i^{n+1} - \frac{k\triangle t}{\rho c_p \triangle x_i^2} T_{i+1}^{n+1} \tag{4}$$

Table 8: Chariot heat shield requirements.

ID	Requirement
CHAR-HS-01	The heat shield shall protect the Chariot from the temperatures of atmospheric entry.
CHAR-HS-02	Heat shields shall be stackable on top of one another for storage.

Table 9: Material properties of Sigratherm

Sigratherm			
Density (g/cmˆ3)	Young's Modulus (GPa)	Bending Strength (MPa)	Thermal Conductivity
0.15	0.25	1.2	0.22

Table 10: Heat Shield Properties.

Mass(kg)	Diameter (m)	Thickness (m)
156.7336	1.849485	0.109743

4.5 Chariot Solid Rocket Boosters

The Chariot's retrograde burn is completed by a pair of "BSB-004a1" solid rocket boosters, illustrated in Fig. 9. These boosters run on Ammonium Nitrate propellant; This propellant has a relatively low ISP but produces nontoxic exhaust, ensuring crew safety [14]. The boosters are rotated 45 degrees inwards so their thrust point towards the center of mass.

Table 11: Chariot booster requirements.

ID	Requirement
CHAR-BSB-01	The solid rocket boosters shall maintain stable conditions in storage for 5 months.
CHAR-BSB-02	The boosters shall not leak toxic dust or gases into the ITM while in storage.
CHAR-BSB-03	The booster propellant shall not include high explosives such as HMX.
CHAR-BSB-04	The boosters shall have clearly marked mounting points on the Chariot to remove the chance of improper installation and angling.

4.5.1 Chariot Solid Rocket Boosters Trade Studies

The team chose from a list of solid rocket propellants provided by Sutton and Bilbarz's "Rocket propulsion Elements [14]." The 45 degree tilt was implemented to impart thrust directly through the center of mass.
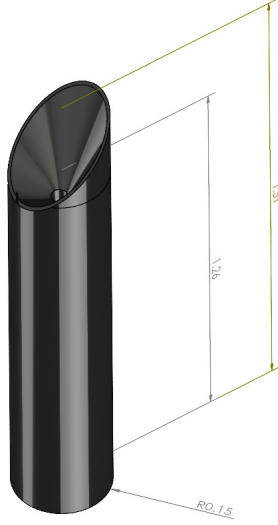
Figure 9: BSB-004a1 Solid Rocket Motor.

Table 12: BSB-004a1 Booster Properties.

Propellant	ISP	Propellant Mass
Ammonium Nitrate	180	116.1 kg
Diameter	**Grains Length**	**Total Mass**
0.3 m	1.26 m	139.3 kg
Tilt Angle	**Total Length**	
45 degrees	1.51 m	

This means that one booster firing will not impart any angular momentum, allowing for more leniency towards possible thrust instability. The farther back the boosters are, the less the tilt has to be; 45 degrees was the minimum to allow the boosters and Chariot to fit within the ITM airlock, which has 2.1 meters of space in length, width, and height.

4.5.2   Storage Safety

The boosters will be stored inside the ITM and will be handled by the crew without full-body protection. As such, the risk of toxicity and ignition must be minimized. Provisions mostly took place in the choice of propellant. High-performance motors could have specific impulse (I_{sp}) of around 265. However, such motors make use of high explosives such as HMX are classified as Class 1.1 explosives[14]. Such an explosive risk was deemed unacceptable to the crew. The next choice examined was Composite AP, Al, and PBAN binder, which maintained an I_{sp} of 260 and was a Class 1.3 explosive, meaning it did not pose a mass detonation

risk [15]. However, the exhaust and burn-rate modifiers are toxic, prompting the team to look into nontoxic alternatives. Ammonium Nitrate with a binder has an I_{sp} of 180, but produces low smoke and nontoxic exhaust. In addition, the propellant is labeled as being neither Class 1.1 nor Class 1.3 and burns slowly [14].

Besides the design of the booster itself, the risk and danger of ignition can also be mitigated by using hand tools that do not produce sparks and specially training the crew to avoid ignition hazards.

4.5.3 Spin Stabilization

The group created a SIMULINK model which heuristically represents the Chariot in EDL configuration as a moment of inertia matrix.

- The x-axis is parallel to the line between the two boosters' attachment points and goes through the center of mass.

- The y-axis goes from the back to the front of the balloon.

- The z-axis completes the right-hand system.

Two thrust vectors represent the boosters, tilted at 45 degrees from the z-axis in opposite directions. Impulse, thrust, and burn times can then be implemented, and the resultant ΔV can be mapped. Figure 10 shows the results of a worst-case scenario where one booster fires with 80% instantaneous thrust and 2 seconds late.
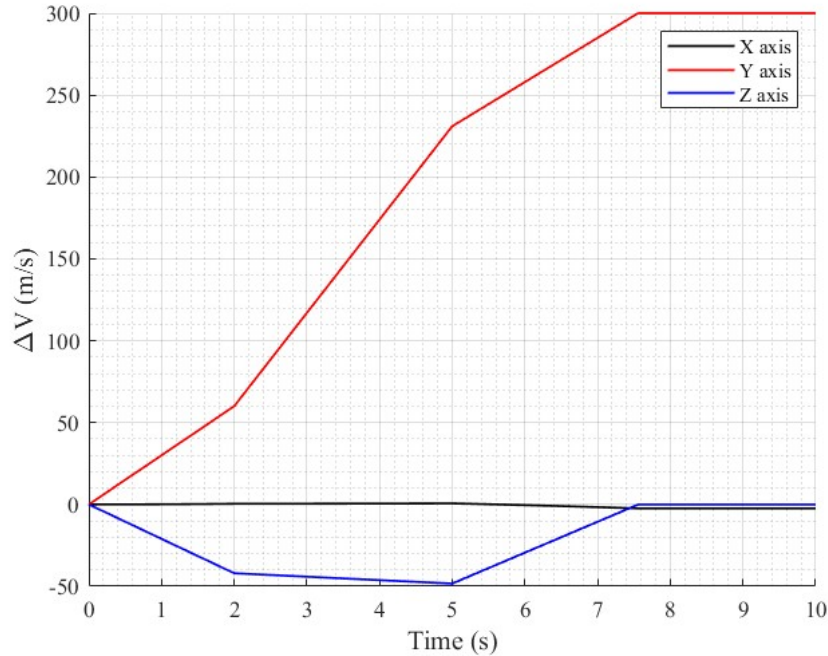
Figure 10: Chariot SIMULINK ΔV over time with one booster firing 2 seconds late at 80% thrust.

4.6   Chariot Attitude Determination and Control Systems (ADCS)

To keep the Chariot pointing retrograde before its deorbit burn, the Chariot utilizes four commercial off-the-shelf (COTS) reaction wheels: Blue Canyon RW4s [16]. The key parameters associated with these reaction wheels are captured in Table 14 along with how they influence the various slew capabilities of the entire Chariot vehicle.

Table 13: Chariot ADCS requirements.

ID	Requirement
CHAR-ADCS-01	The ADCS shall allow the Chariot to maintain a retrograde pointing direction for its descent.
CHAR-ADCS-02	The ADCS shall fit as a self-contained system on the Chariot on the descent configuration.
CHAR-ADCS-03	The ADCS shall be detached from the vehicle after atmospheric entry and before scientific operations begin.

Table 14: RW4 Reaction Wheels Specifications and Chariot Slew Characteristics

RW4 Specs	Value
Max spin (RPM)	4000
Momentum storage (Nms)	4
Max torque (Nm)	0.25
Moment of inertia (kgm^2)	0.0095

Chariot Slew Characteristics	Value
Center of Mass (mm)	[-386.33, 0, 30.28]
Moment of inertia (kgm^2)	$\begin{bmatrix} 90.6480 & 0 & 0 \\ 0 & 8.8577 & 0 \\ 0 & 0 & 40.9140 \end{bmatrix}$
Max z-axis slew rate (deg/s)	5.60
Max y-axis slew rate (deg/s)	25.85
Max x-axis slew rate (deg/s)	2.53

4.7 Probe Entry, Descent, and Crash (EDC)

The probe will also burn 300 m/s to descend into the atmosphere, but has less stringent pointing requirements. The probe only needs to burn into a suborbital trajectory and avoid missing Venus. Thus, it can tolerate more angular deviation during the re-entry burn and does not require an ADCS module, simplifying the mission architecture.
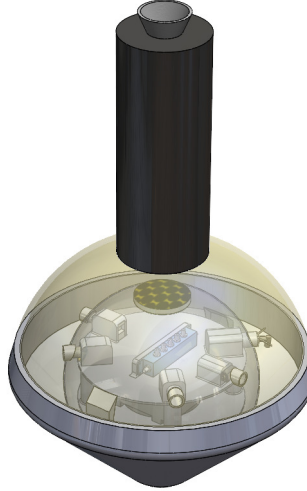
Figure 11: Static Drop in EDC configuration.

Table 15: Static drop probe EDC requirements.

ID	Requirement
PRO-EDC-01	The probe shall free fall through Venus' atmosphere for data collection.
PRO-EDC-02	The probe shall burn 300 m/s retrograde, with a tolerance of 5%.

4.8 Probe Solid Rocket Motors

The probes use one BSB-005a1 solid booster, installed directly opposite the heat shield. This booster is similar to the BSB-004a1 of the Chariot but 1/10 of the mass due to the lack of need to tilt as well as the total carried payload of the Chariot (heat shield, reaction wheels, Chariot vehicle) being 297 kg while the static drop is 60 kg. The booster will mechanically separate from the static drop after the burn is complete and will drift away from the probe before atmospheric entry.
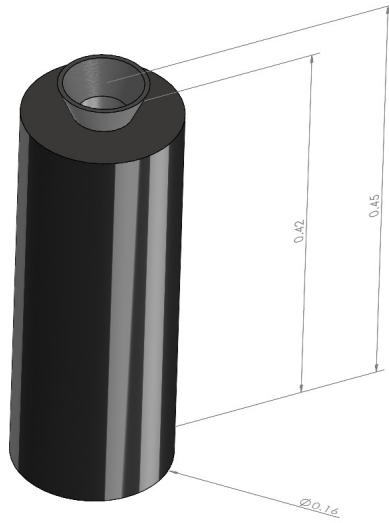
Figure 12: BSB-005a1 Solid Rocket Motor.

Table 16: BSB-005a1 Booster Properties.

Propellant	ISP	Propellant Mass
Ammonium Nitrate	180	11.5 kg
Diameter	**Grains Length**	**Total Mass**
0.16 m	0.42 m	13.9 kg
Tilt Angle	**Total Length**	
0	0.45 m	

5 The Interplanetary Transfer Module (ITM)

5.1 ITM Requirements

RHEIA^2's Interplanetary Transfer Module (ITM) is designed to meet the storage, assembly, and deployment demands of the science payloads. The module delivers an organized workspace for astronauts to assemble the Chariots, with numerous drawer compartments for tools and components. During Chariot assembly, astronauts will utilize hooks, straps, and footholds in the module to fasten large components in the workspace. For payload deployment of the static probes and Chariots, astronauts will operate the ITM's integrated airlock with a linear actuator mechanism. Table 17 displays the full system requirements of the Interplanetary Transfer Module.

Table 17: Full system requirements of the Interplanetary Transfer Module.

ID	Requirement
RHEIA^2-ITM-01	The ITM shall withstand launch and LEO environmental conditions.
RHEIA^2-ITM-02	The ITM shall store all the components necessary for the assembly of the Chariots.
RHEIA^2-ITM-03	The ITM shall autonomously dock with the Deep Space Transport in LEO.
RHEIA^2-ITM-04	The astronauts shall assemble the Chariots in the ITM.
RHEIA^2-ITM-05	The fully assembled Chariots shall be deployed from the ITM.
RHEIA^2-ITM-06	The static probes shall be deployed from the ITM.

5.2 ITM Trade Studies

Subsystems for the Interplanetary Transfer Module were designed to provide for the mission demands on the module, primarily during LEO transit to docking with the Deep Space Transport. In addition, subsystems such as ECLSS, airlock/payload deployment, and the internal structural configuration were designed to provide astronauts the workspace environment they needed for assembling the Chariots. During LEO transit, the ITM will utilize Attitude Determination and Control, Structures, Power, Thermal Control, Communications, and Command and Data Handling subsystems to mitigate LEO environmental impacts on the module and ensure successful docking with the Deep Space Transport. Upon docking, the ITM will begin to draw resources - such as power, thermal control, propulsion, and ECLSS - from the Deep Space Transport for the remainder of the mission. The designed ECLSS subsystem will provide astronauts a safe workspace environment for payload assembly and the payload deployment systems will allow for effective deposition of the Chariots and static probes into the Venusian atmosphere for data collection. Table 18 shows the final mass, volume, and power budgets for the ITM's subsystems and overall configuration. A 10% contingency and 25% margin were used in the calculations.

Table 18: Final system budgets for the Interplanetary Transfer Module.

	Structures	TCS	ADCS	TMTC	ECLSS	Payloads	Power	Total	With Contingency	Allocated
Mass (kg)	10049.6	146.4	83.6	19.3	132.0	2864.3	253.2	13295.2	14624.7	18280.9
Volume (m^3)	6.8	1.8	0.04	0.03	1.37	60.5	0.05	70.6	77.7	97.1
Power (W)	-	-	945.1	86.0	-	-	-	1031.1	1134.2	1417.7

Ultimately, RHEIA^2's ITM and its subsystems deliver an innovative workspace and storage solution to meet the mission's requirements and functionality. With human-centric in-space manufacturing and assembly as the primary design consideration, the ITM acts as the forefront modular spacecraft for manned deep-space science missions. Fig. 13 displays the full ITM system with its subsystem designs and cargo.
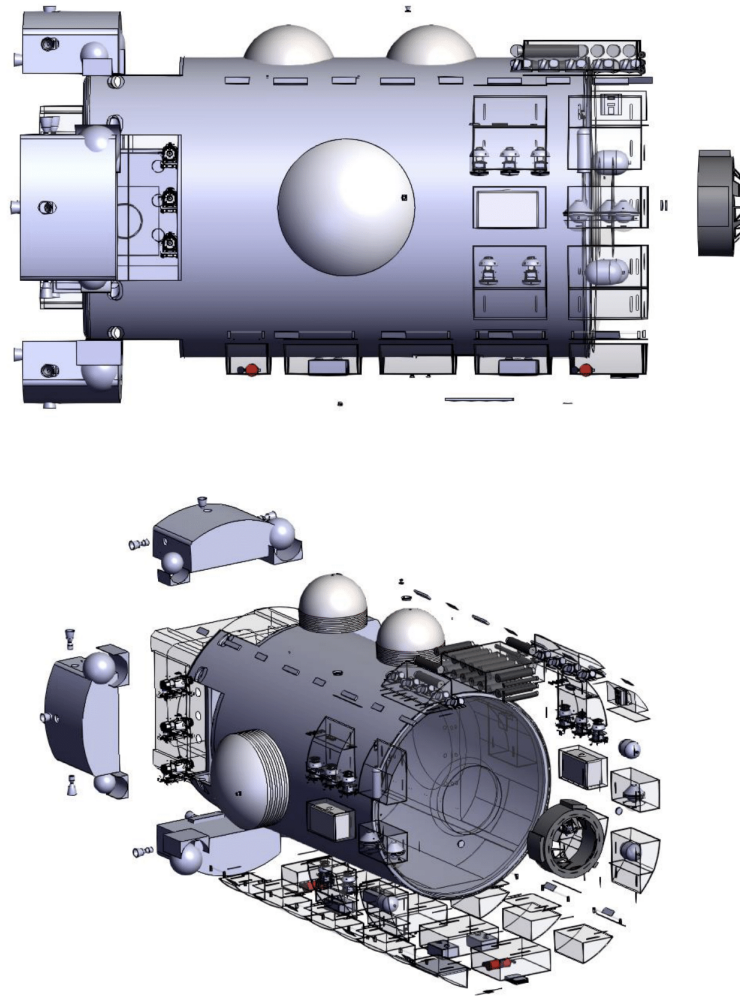

Figure 13: Exploded view of the ITM assembly.

5.2.1 Environmental Control and Life Support System (ECLSS)

The RFP calls for a crew of four to fulfill the robotic science mission needs. Thus, the critical purpose of the ITM is to provide support for two crew members at a time to perform manufacturing and assembly of the Chariots. While the assembly or payload deployment process is occurring inside the ITM, the remaining two crew members will perform monitoring operations of the deployed Chariots and data analysis inside the DST. The ITM was designed with the following ECLSS requirements adapted from the NASA STD 3001 Vol 2 [17] to accomplish this purpose, with the assumption that the DST's ECLSS is modeled after the ISS.

Table 19: ECLSS requirements of the Interplanetary Transfer Module.

ID	Requirement
ITM-ECLS-01	The pressurized chamber of the ITM shall have partial pressures of O_2 in the range of 19.5-23.1 kPa.
ITM-ECLS-02	The pressurized chamber of the ITM shall have partial pressures of CO_2 less than 0.4 kPa.
ITM-ECLS-03	The pressurized chamber of the ITM shall have partial pressures of N_2 in the range of 77.3-79.5 kPa.
ITM-ECLS-04	The relative humidity in the ITM shall remain within the range of 30% to 70%.
ITM-ECLS-05	The air in the ITM shall flow inside the pressurized chamber within the range of 0.08-0.2 m/s.
ITM-ECLS-06	The habitable pressurized volume of the ITM shall be at least 20 m^3 to accommodate two crew members.

The DST will centrally provide the main ECLSS subsystems to the ITM after docking. These subsystems include the pressure control system, oxygen generation assembly, carbon dioxide removal assembly, thermal control system, and trace contamination control. The DST will provide power to the ITM to support its ECLSS, estimated to be a power draw of 0.21 kW. The ITM itself will include the following ECLSS subsystems: atmosphere pressure control, temperature and humidity control, air contamination control, fire detection and suppression, and human support systems. Through performing trade studies on previous ISS modules, such as the European Space Agency's Columbus module [18] and the Japanese Aerospace Exploration Agency's Kibo module [19], we determined the essential components necessary to support each ECLSS subsystem within the ITM.

5.2.1.1 Atmosphere Pressure Control & Air Contamination Control The table below lists the NASA STD 3001 Vol 2 [17] standardized atmospheric composition of the ISS and the chosen atmosphere for the ITM pressurized crewed chamber. Similar to the ISS, the total pressure of the ITM will be 101.3 kPa, which resembles Earth sea level conditions.

The atmospheric conditions chosen for the ITM were determined through trade studies on the ISS atmosphere and analysis on the most optimal conditions for astronauts to conduct in-space assembly operations. This includes providing the crew a "shirt-sleeve" temperature within the ITM and ensuring that the atmospheric pressure is controlled. The ITM will contain four valves on the lower side of the forward (docking adapter) end and three pressure sensors to monitor the atmospheric pressure and circulate air throughout the

ITM. Furthermore, three Bacterial Filter Elements (BFE) HEPA filters will be used for air contamination control, with two filters located at the forward end and one located at the back (airlock) end of the ITM.

Table 20: Chosen atmospheric pressure control components for the ITM.

Component	NASA Standard	ITM
pO_2	19.5-23.1 kPa	21 kPa
pCO_2	<0.4 kPa	0.267 kPa
pN_2	77.3-79.5 kPa	78 kPa
Humidity	30-70%	60%
Temperature	18-24°C	22°C
Airflow	0.08-0.2 m/s	0.08-0.2 m/s

Cabin Fan
Assembly

Inside of Docking
Adapter

IMV Air
Outlet to DST

IMV Air Inlet
from DST
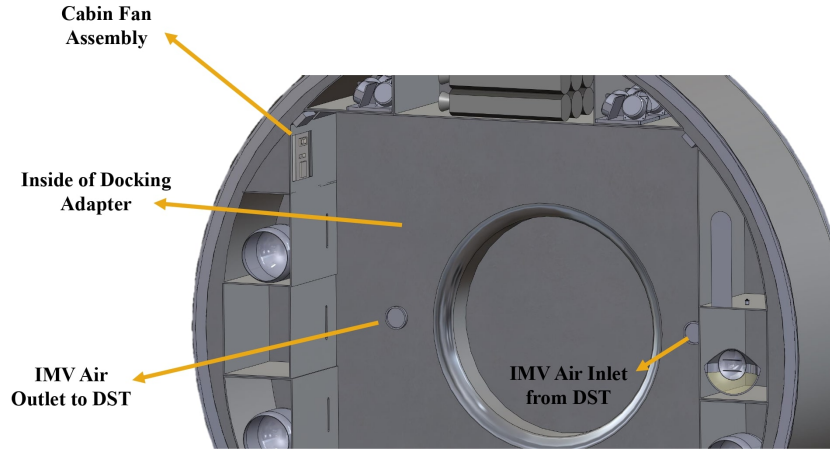
Figure 14: Interior view of the docking adapter wall, including the cabin fan assembly and IMV air inlet and outlet.

The ITM will also contain a commercial, off-the-shelf air tank, the Luxfer S106W, as a safety precaution in the event of a small helium leak due to the helium tanks onboard. The Luxfer S106W air tank has previous spaceflight heritage on the ISS, as they were sent to the ISS on a resupply flight in 2021 [20]. An oxygen detector is included to measure oxygen levels and identify signs of oxygen deprivation or loss in the atmosphere. If a helium leak does occur, astronauts are advised to open the compartment that contains the air tank and connect it to a feed line through an emergency valve located near the docking adapter. A pressure regulator will be used to control and adjust the pressure of the air being drawn from the air tank. The specifications of the Luxfer S106W air tank [21] are listed below.

Table 21: Luxfer S106W air tank specifications.

Specification	Value
Volume	0.018 m^3
Service Pressure	300 bar
O$_2$	21%
N$_2$	78%
Mass (gas and tank)	28.76 kg
Material	Composite Cylinder
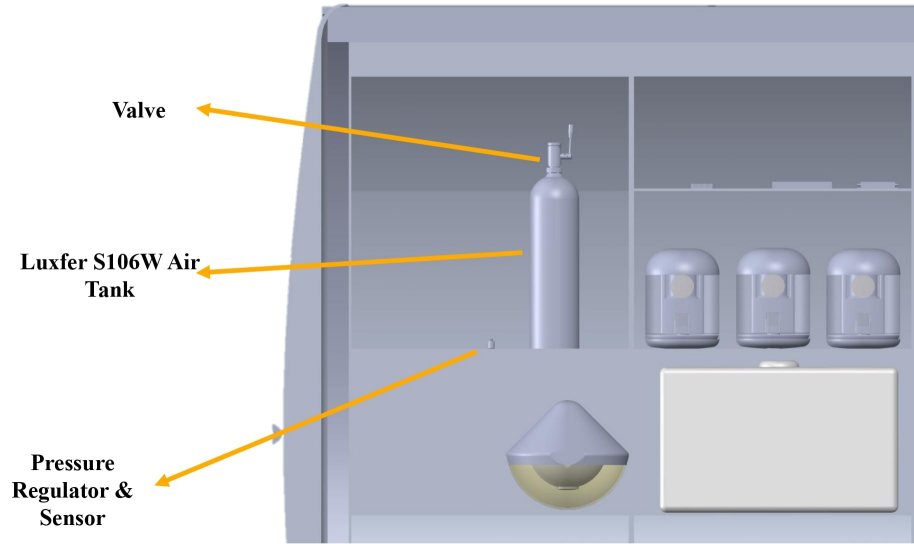
Figure 15: Luxfer S106W air tank with pressure regulator and valve inside an ECLSS compartment near the docking adapter.

5.2.1.2 Temperature and Humidity Control The ITM will contain an Inter Module Ventilation (IMV) supply, consisting of valves and fans, that will be connected to the main DST ECLSS to provide air into the module. The IMV will be located on the forward end, on the face of the docking adapter. The cabin fan assembly will also be located at the forward end near the IMV. There will be eight diffusers located along the upper cabin, with four diffusers on each side of the ITM. Additionally, there will be four air inlets on each lower side of the ITM. Lastly, three temperature and humidity sensors will be located throughout the ITM to provide constant monitoring and control of these atmospheric variables.
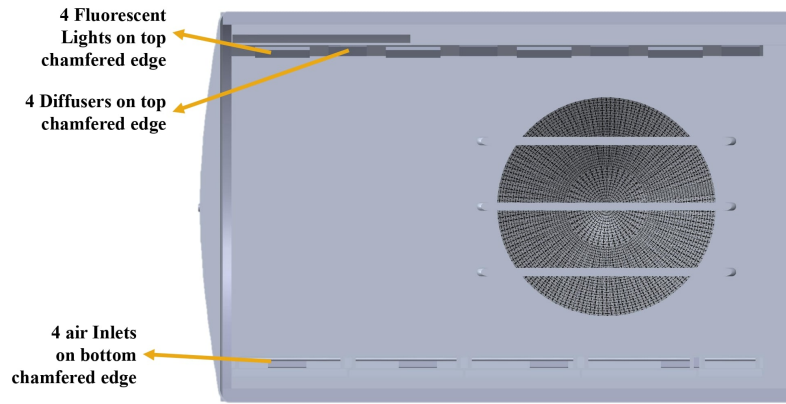
Figure 16: Side wall view of the ITM, with fluorescent lights, diffusers, and air inlets on the edges.

5.2.1.3 Fire Detection and Suppression The ISS uses portable CO_2 fire extinguishers in the U.S. modules as they are the most effective against sensitive electronics [22]. Following the NASA requirement that each module should have at least two fire extinguishers, our ITM will contain one fire extinguisher at the forward end and the other at the back end. The ITM will also house two smoke detectors that will continuously monitor the air and serve as the fire detection and warning system. In the event of a fire, the IMV will automatically cease operations to prevent further spread, and astronauts will be required to wear oxygen masks before suppressing the fire.

5.2.1.4 Human Support Systems To support the crew and their manufacturing operations, we will have eight total fluorescent lights, four located along the upper cabin on each side that alternate with the diffusers. Additionally, the crew will have four HP ZBook 15 laptops inside the ITM, which are currently used on the ISS, to assist with data processing and monitoring of the Chariots and operating the airlock.

Figure 17: Fire extinguishers and laptops located in ECLSS compartments on the bottom surface of the ITM.

5.2.2 Attitude Determination and Control Systems (ADCS)

The ADCS subsystem for the ITM has the following system requirements from launch until docking with the DST. Once docked, the ADCS subsystem for the ITM is no longer required and the primary purpose of the ITM is to provide ECLSS, payload development, and safe space for in-space manufacturing and assembly.

Table 22: ADCS System Requirements.

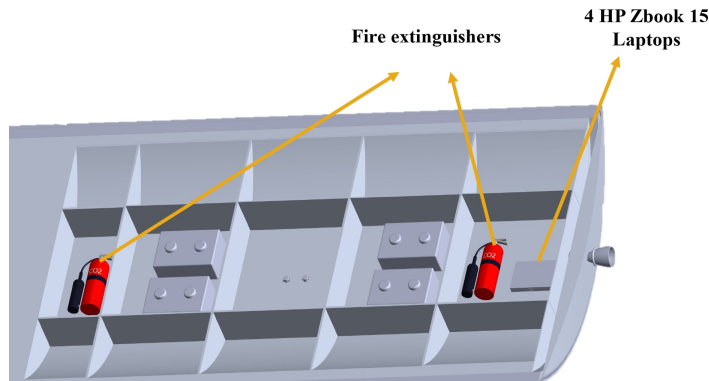| ID	Requirement
ITM-ADCS-01	The ITM's ADCS system shall enable three-axis stabilization.
ITM-ADCS-02	The ITM's ADCS system shall have a minimum accuracy of $0.01°$ to facilitate docking.
ITM-ADCS-03	The ITM's ADCS system shall have the capability to conduct rapid rendezvous and docking maneuvers within 2 days.
ITM-ADCS-04	The ITM's ADCS system shall have the capability to close in at a rate below 0.5 m/s during initial docking.
ITM-ADCS-05	The ITM's ADCS system shall have the capability to close in at a rate below 0.05 m/s during final docking.

To meet the requirements in the table throughout the 2-day rendezvous and docking with the DST, the Attitude Determination and Control System (ADCS) of the Interplanetary Transport Module (ITM) employs a layered approach (with multiple system redundancies) to ensure precise attitude control and navigational accuracy throughout its operations. Central to the ADCS are the Inertial Measurement Unit (IMU) and Inertial Navigation System (INS), which play critical roles in quickly determining the spacecraft's attitude by sensing linear accelerations and angular velocities. Here, the INS adds additional capability by including a GPS module which provides additional position information in orbit above Earth. These systems provide the fundamental real-time trajectory and attitude information necessary for the initial phases of launch and are indispensable during periods when other navigational aids may be compromised by external factors like direct sunlight or other bright celestial bodies. However, the IMU and INS are subject to drift and need to be augmented by external sensors. As such, augmenting the IMU and INS, the ITM's ADCS architecture integrates three high-precision star trackers for fine attitude determination. These sensors allow the ITM to attain the $0.01°$ pointing accuracy requirement during docking maneuvers. Star trackers, in particular, are a popular choice on larger spacecraft and are present in the ADCS architectures of many vehicles that fly to the ISS including the SpaceX Dragon capsule. Unfortunately, the star trackers are not sufficient for high-rate slew maneuvers (especially those performed during an emergency). To account for this and provide additional redundancy, the ITM ADCS also includes an Earth Horizon sensor. The placement of all of these sensors are shown in Figures 18, 19, and 20.
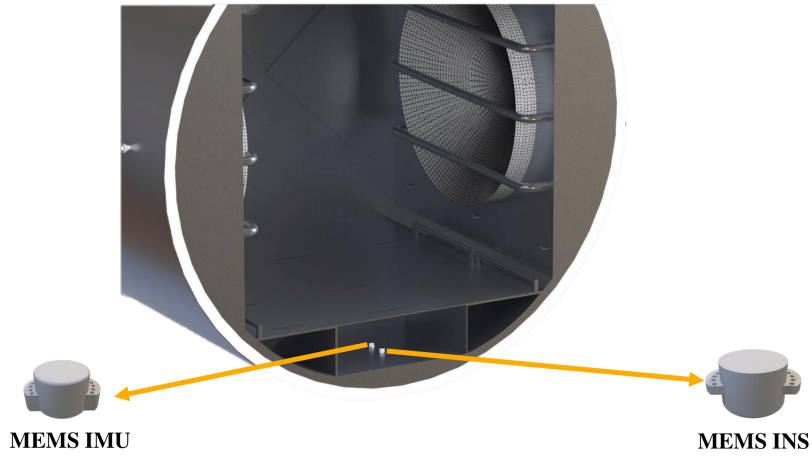
Figure 18: IMU and INS Placement in ITM Interior Compartment
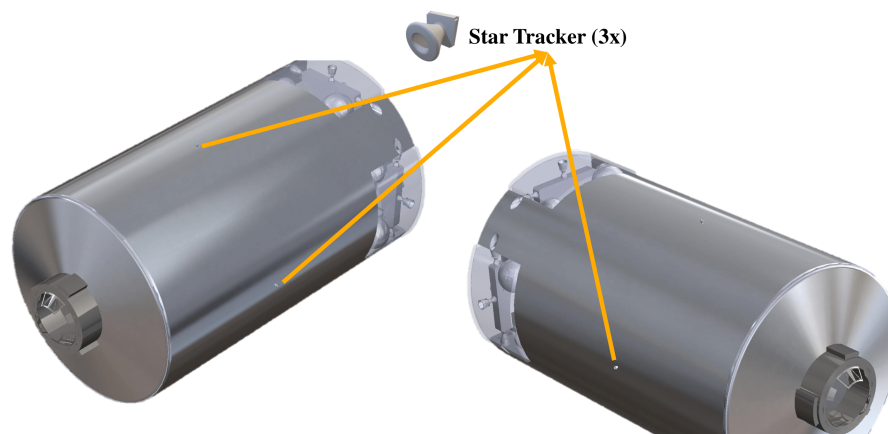
Figure 19: Triple star tracker placement on ITM Body
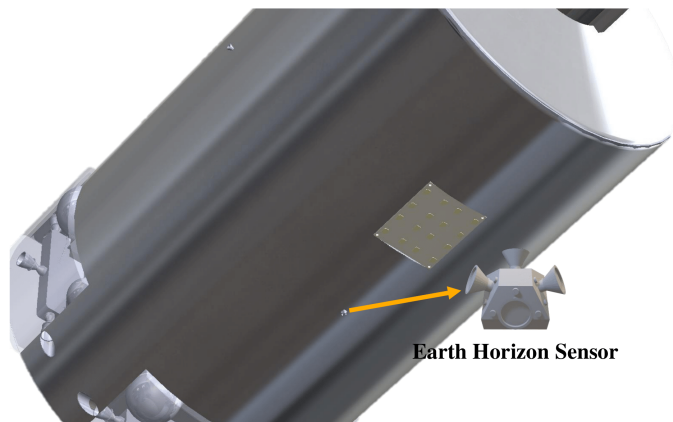
Figure 20: Earth Horizon Sensor placement on bottom of ITM Body along with ground-station patch antenna

The sizing and placement of these sensors were determined based on the ADCS parameters and disturbances derived from CAD and formulas relating to aerodynamics, gravity gradient, and rigid body rotation. Internal torques are primarily derived from thruster firings while external torques are present from orbital drag, gravity, and solar radiation. These parameters are captured in Table 23.

Table 23: ITM Disturbance Quantification and Key Inertia parameters

Parameter	Value
Torque Sources	
Internal (Slew Maneuvers)	773.500 Nm
External (Gravity Gradient)	5.06e-2 Nm
External (Aerodynamic Drag)	2.71e-4 Nm
External (Solar Radiation Pressure)	1.67e-4 Nm
ITM Inertia Information	
Center of Mass (COM)	$[-775.70, 129.00, 37.1]$ mm
Principal Moment of Inertia Matrix I	$\begin{bmatrix} 46733.84 & 0 & 0 \\ 0 & 64469.82 & 0 \\ 0 & 0 & 77045.23 \end{bmatrix}$ kgm^2
Total Mass	13295.21 kg

Lastly, propulsion is delivered through four modules shown in Figures 22 and 23, each with four 445N thrusters, providing both orbital and fine attitude maneuverability, inspired by the Saturn V's auxiliary propulsion module. The decision to use only thrusters and forgo other hardware like reaction wheels was made considering the short ADCS operational timeline (2 days) and aligns with the ADCS operational paradigms of both the SpaceX Dragon and Boeing Starliner, favoring thrusters over alternative actuators for the brief ADCS operational window. Importantly, the propulsion system employs ASCENT propellant, preferred over traditional options like hydrazine, due to its non-toxicity—a crucial consideration for crew safety and payload integrity. ASCENT's selection underscores an inherent mission commitment to minimizing toxicological risks in human-rated missions, aligning with modern trends in spaceflight safety. A piping and instrumentation diagram (or P&ID) for the propulsion module is shown in Fig. 21.

Figure 21: ASCENT Propulsion Module P&ID Diagram

Figure 22: ASCENT Propulsion Module Layout
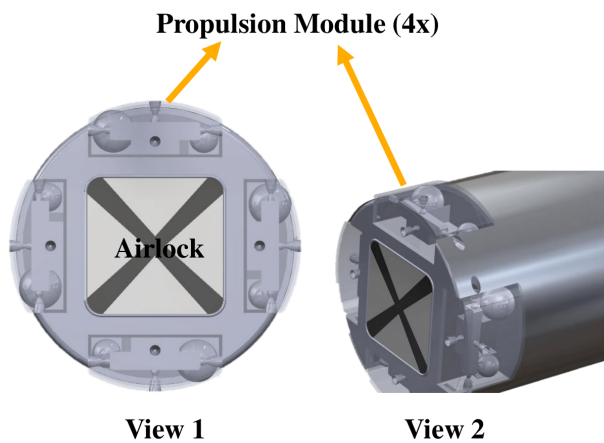
Figure 23: Propulsion Module Location on ITM

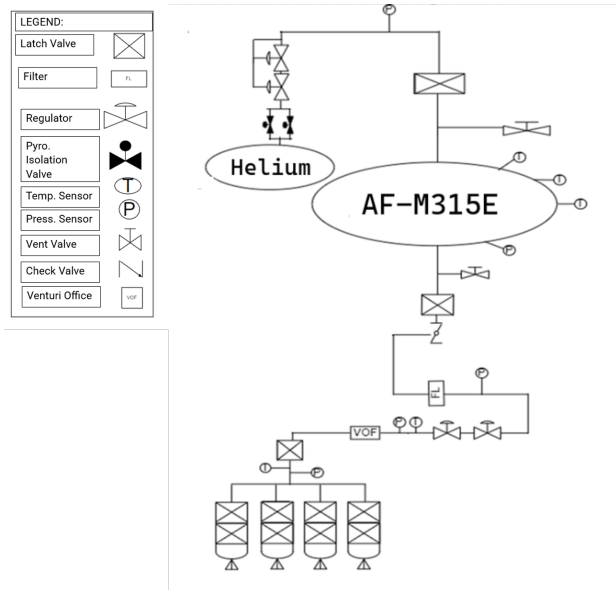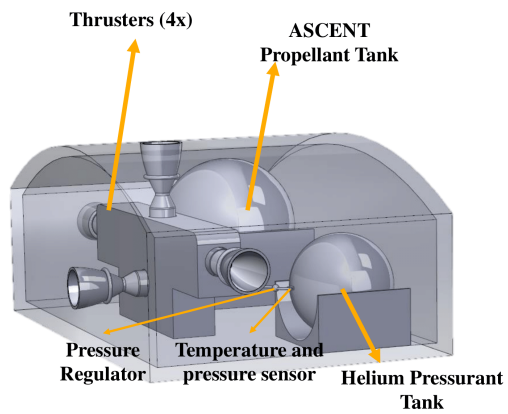Sizing of the propellant and pressurant tanks, assumed to be thin spherical tanks, was conducted after the rendezvous and docking simulation, which provided the required δV for the maneuvers that the ITM will need to undergo. Following this, the propellant mass for the ADCS maneuvers was determined through a MATLAB script implementing Tsiolkovsky rocket equation

$$m_{\text{propellant}} = m_{\text{dry}} \left(e^{\frac{\Delta V}{I_{\text{sp}} g_0}} - 1 \right) \tag{5}$$

Here, m_{dry} is the dry mass of the spacecraft, ΔV is the change in velocity, I_{sp} is the specific impulse of the propulsion system, and g_0 is the standard acceleration due to gravity.

Through this equation, the total δV required for the mission, $\Delta V = 169.75$ m/s, and the specific impulse of the ASCENT chemical propulsion system, $I_{sp_{chem}} = 262.08$ s, was used to calculate the propellant mass. For propellant tank sizing, the script accounted for the density of the ASCENT propellant (1460 kg/m^3) and incorporated additional volume considerations for ullage, propellant management devices (PMDs), residuals, and reserves. The total volume, V_{total}, was then used to deduce the necessary tank dimensions and material requirements for a Titanium-based structure (Ti-6Al-4V); titanium is a widely used material for space propellant/pressurant tanks. The structural integrity under pressure was ensured by sizing the tank walls to withstand a burst pressure, which was calculated with a safety factor of *3* applied to the operational pressure. The pressurant, Helium in this case (typical for ASCENT propellant systems), was sized iteratively to maintain proper tank pressure throughout the mission, considering isentropic relationships such as

$$P_2 = P_1 \left(\frac{V_1}{V_2} \right)^{\gamma}, \tag{6}$$

where P represents pressure, V volume, and γ the heat capacity ratio for helium. This iterative calculation balanced the initial and final pressurant states, accounting for thermodynamic properties and the material characteristics of the tank. The results of this parametric calculation are captured in Table 24 and Table 25.

Table 24: ASCENT Propellant Tank Parameters

Tank Parameter	Value
Propellant Mass (kg)	212.36
Tank Volume (m^3)	0.196
Tank Radius (m)	0.36
Expected Operating Pressure (MPa)	2.07
Tank Burst Pressure (MPa)	4.14
Tank Wall Thickness (mm)	0.785
Tank Mass (kg)	6.82
Material	Titanium: Ti-6Al-4V

Table 25: Helium Pressurant Tank Parameters

Tank Parameter	Value
Converged Pressurant Mass (kg)	0.50
Tank Volume (m^3)	0.047
Tank Radius (m)	0.25
Expected Operating Pressure (MPa)	6.21
Tank Burst Pressure (MPa)	18.62
Tank Wall Thickness (mm)	2.30
Tank Mass (kg)	9.33
Material	Titanium: Ti-6Al-4V

5.2.3 Docking

The design philosophy for the docking system of the Interplanetary Transport Module (ITM) is based on system simplicity and reliability. Opting for a passive docking adapter on the ITM significantly reduces the complexity of the system, delegating more sophisticated active docking responsibilities to the Deep Space Transport (DST). The DST's active docking adapter is equipped with advanced LIDAR, cameras, and other sensors to facilitate precise docking maneuvers per the ISS docking standard. Upon successful docking, the passive adapter on the ITM integrates seamlessly with the DST, facilitating the transfer of electrical power and critical ECLSS components, including atmospheric gases. This integration ensures the ITM leverages the DST's robust support systems, streamlining the ITM's design and enhancing the mission's overall efficiency. A detailed CAD model of the docking adapter is attached to the front of the ITM as shown in Fig. 24.
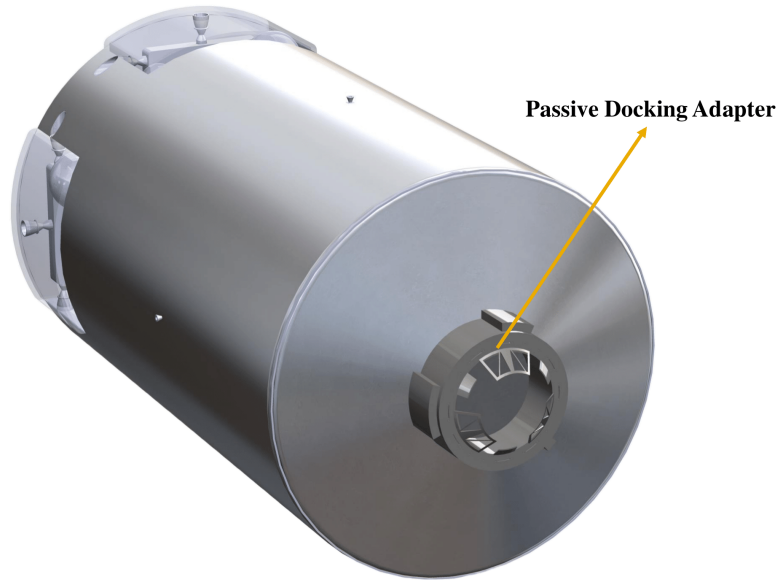

Passive Docking Adapter

Figure 24: Passive Docking Adapter Design and Location on ITM

5.2.4 Structures

Table 26 displays the ITM's structural requirements to meet the mission's structural and configuration demands on the module.

Table 26: Structural requirements of the interplanetary transfer module.

ID	Requirement
ITM-STR-01	The ITM's structures shall withstand 6 g's of axial acceleration and 2 g's of lateral acceleration during launch.
ITM-STR-02	The ITM's structures shall withstand the launcher's peak vibration frequency of 35 Hz.
ITM-STR-03	The ITM's structures shall withstand a critical buckling load of 52.6 MN during launch.
ITM-STR-04	The ITM's structures shall have axial and lateral load natural frequencies of more than 70 Hz.
ITM-STR-05	The ITM's structures shall withstand a pressure differential between internal atmospheric pressure and external vacuum.
ITM-STR-06	The ITM shall provide 61 m^3 of internal storage capacity for payloads, assembly components, and subsystem components.
ITM-STR-07	The ITM's structures shall provide meteorite and debris protection against the environments of LEO, Venus transit, and Venus orbit.

Launch load cases were the main design considerations with the ITM's primary structure. Additionally, the primary structure needed to withstand the approximate 1 atm pressure differential in the space environment. In sizing the ITM's primary structure, compression, buckling, and rigidity load cases based on launch conditions were considered. A thorough material selection process was conducted to compute these load cases and size the primary structure to withstand the launch environment.

Aluminum alloys are the most common material used in spacecraft structures due to an optimal combination of high strength-to-weight ratio and manufacturability [23]. Specifically, Aluminum 6061 and 2024 alloys are among the most popular materials in spacecraft structures [23]. Additionally, Aluminum 2219 is a popular structure and shielding material that has been employed on module and orbital vehicles, such as ESA's Columbus ISS module and ATV [24]. Aluminum 2024 alloy was chosen as the ITM's primary structure material for its superior strength and mechanical properties. Table 27 draws comparisons in mechanical properties between the different Aluminum alloys considered for the ITM's primary structure [25].

Table 27: Material properties of aluminum alloys, with u denoting ultimate strength and y denoting yield strength.

	Al-6061	Al-2024	Al-2219
Tensile Strength	310 MPa (u) 276 MPa (y)	440+ MPa (u) 290 MPa (y)	400 MPa (u) 290 MPa (y)
Elastic Modulus	68.9 MPa	73.1 MPa	73.1 MPa
Fatigue Limit	97 MPa	138 MPa	103 MPa

The thickness sizing of the ITM's Aluminum 2024 primary structure was derived from the compression, buckling, and rigidity launch load cases and the pressure differential load case in space. The compression launch loads and launch vehicle natural frequency were derived from SpaceX's Falcon User Guide [2]. The buckling launch loads were calculated using the beam equation

$$P_{\text{cr}} = \frac{\pi^2 EI}{(L')^2}, \tag{7}$$

where P_{cr} is the critical buckling load for a beam, E is the elastic modulus of the structural material, I is the second moment of inertia, and L' is the effective length of the structure. The rigidity launch loads were calculated using the equations

$$f_{\text{n,a}} = 0.25\sqrt{\frac{AE}{mL}}, \tag{8a}$$

$$f_{\text{n,l}} = 0.56\sqrt{\frac{EI}{mL^3}}, \tag{8b}$$

where $f_{\text{n,a}}$ is the axial natural frequency, A is the cross-sectional area of the beam, E is the material's elastic modulus, m is the material's mass, L is the length of the structure, and $f_{\text{n,l}}$ is the lateral load natural frequency. Finally, the pressure differential loads were calculated using the equations

$$\sigma_1 = \frac{pr}{t}, \tag{9a}$$

$$\sigma_2 = \frac{pr}{2t}, \tag{9b}$$

where σ_1 is the circumferential (hoop) stress, p is the internal pressure, r is the cylinder's radius, t is the thickness, and σ_2 is the axial stress. Because the thickness of the structure is much less than the radius of the structure, these thin-walled cylinder pressure equations were used. For the ITM's primary structure to withstand rigidity launch loads, the axial and lateral natural frequencies must each be at least double the natural frequency of the launch vehicle. Table 28 summarizes the structural load calculations and the required thickness of the primary Aluminum 2024 structure to withstand the load cases. A 1.50 factor of safety was used in the sizing efforts for each load case. From these calculations, the thickness of the ITM's primary structure was finalized as 4.5 mm.

Table 28: Required structural thicknesses by load case.

Load Case	Value	Required Thickness
Compression	Axial: 6 g Transverse: 2 g	<1 mm
Buckling	$P_{\text{cr}} = 52.6$ MN	<1 mm
Rigidity	$f_{\text{n, launcher}} = 35$ Hz	4.5 mm
Pressure	$\sigma_y = 290$ MPa	1 mm

In addition to the ITM's primary structure, a meteorite and debris protection shield was designed to mitigate impact and radiation risks in the space environment. It was assumed that the DST would employ active radiation shielding methods that are currently being considered for manned deep-space missions [26]; therefore, the ITM's MDPS was designed primarily for LEO transit, the near-Earth space environment, and as a redundant architecture. ISS modules commonly employ a Stuffed Whipple configuration for their MMOD shields with an outer bumper of aluminum material, MLI, and a protective material like Nextel or Kevlar [27]. The standoff distance between the outer bumper and the primary structure is typically between 10-30 cm [27] for ISS modules. For the protective material within the Stuffed Whipple MDPS, polyethylene and Kevlar were considered for their radiation and impact protection properties. Polyethylene has great radiation shielding properties [28] and significantly favorable density over Kevlar; however, Kevlar was chosen for the MDPS structure because it could withstand the rigidity launch loads much more favorably than polyethylene. The final MDPS structural configuration has a 10.25 cm standoff with - from outermost layer to innermost layer - a 0.3 cm Aluminum 2024 layer, a 2 cm MLI layer, a 7.5 cm Kevlar layer, and the 0.45 cm Aluminum 2024 primary structure layer. Table 29 shows the final masses of the ITM's structural elements.

Table 29: Final masses of the ITM's structural elements.

Component	Mass (kg)
Al-2024 (Outer Layer)	594.0
Kevlar	8537.6
Al-2024 (Inner Layer)	918.0
Total	10049.6

Fig. 25 shows the final sizing of the ITM, designed with storage capacity and workspace volume in consideration. The ITM is also shown in the Falcon Heavy payload volume in Fig. 25. From SpaceX's Falcon User's Guide, the usable payload fairing volume is 4.6 m in diameter and 11.4 m in height.
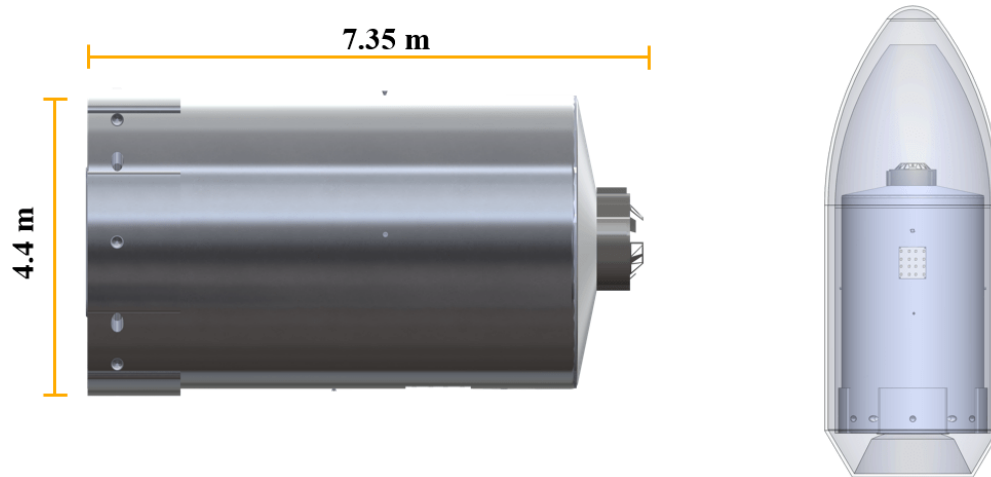
Figure 25: Overall dimensions of the ITM and the ITM configured with the Falcon Heavy payload fairing.

The ITM's internal structure was designed with ease of human assembly and manufacturing as the primary consideration. Importantly, the ITM had to provide 61 m^3 of internal storage capacity for the payloads, assembly components, and subsystem components. The final internal configuration of the ITM derived inspiration from the International Standard Payload Rack design and JAXA's Kibo module [3] for its organization and science rack architecture. Fig. 26 exhibits the ITM's internal storage and labeled components.

1: COPV Helium Tanks
2: Static Drop Probes
3: ECLSS – Air Tank
4: ECLSS – Fire Extinguisher, HP 2book 15 Laptops (x4)
5: Chariot Reaction Wheels
6: Solid Rocket Boosters

7: Chariot – Science Payload Packages
8: Chariot – Water Tanks
9: Primary Batteries
10: Airlock Door
11: Chariot – Balloon Shells
12: Chariot – Heat Shields
13: Footholds
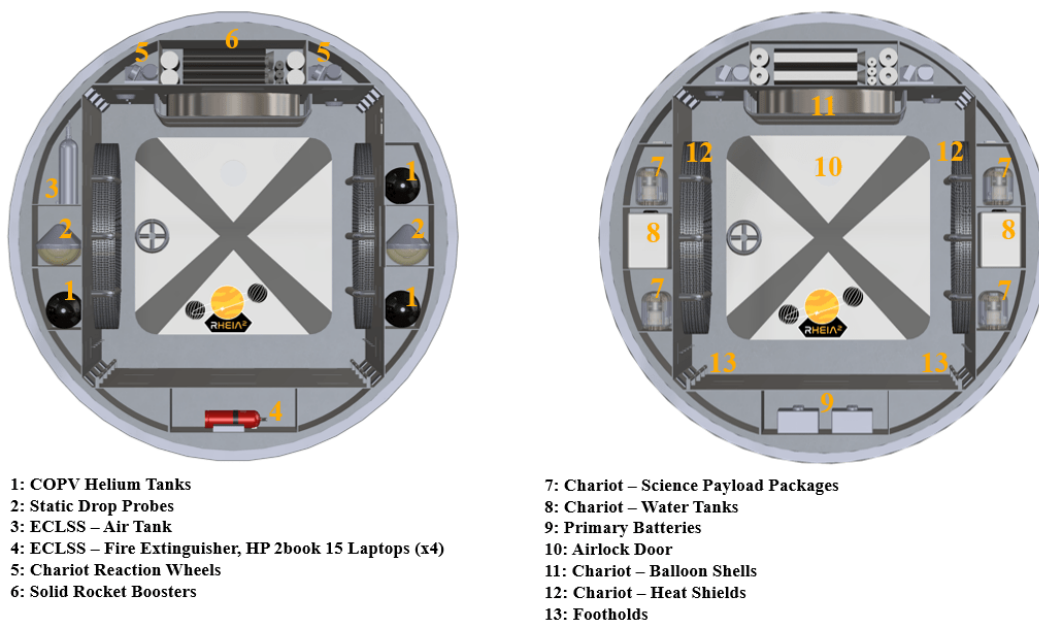
Figure 26: ITM's internal configuration; the left capture displays the drawer units immediately entering the module through the docking interface and the right capture displays the drawer units after the initial units.

The ITM provides a 2.95 m by 2.95 m cross-sectional area for the astronauts' workspace. The drawer compartments displayed in Fig. 26, which open on one of the sides for compartment access, have grooved handles to minimize handle volume. The general compartment configuration in the ITM places some of the bulky Chariot assembly components in the large overheat compartments, the ITM's subsystem components (ECLSS, ADCS, Power) in the bottom floor compartments, and the payload components in the sidewall compartments. The plastic water tanks seen in Fig. 26 were sized to hold 390 kg of water for Chariot assembly, adding approximately 90 kg of water as a contingency. The pressurized helium tanks seen in Fig. 26 were sized to hold 12 kg of helium gas for Chariot assembly, adding approximately 4 kg of helium as a contingency. The tanks are pressurized to 10.3 MPa and were sized with a high safety factor of 3. The helium tanks are 304 stainless steel (1 mm thickness) and Kevlar (3.5 mm thickness) COPVs. This tank architecture was selected with safety and flight heritage in consideration for pressurized gas cylinders aboard the ISS [29] and the Space Shuttle [30], and show promising performance for deep-space missions [31].

As shown in Fig. 26, the Chariot heat shields and balloon shells are fitted into the walls of the ITM and secured by straps for storage. For Chariot assembly, the astronauts will utilize a fastening scheme in which large assembly components will be fastened down to the floor of the ITM with straps connected to hooks lining the sidewalls of the ITM. Fig. 27 illustrates the hooks in the ITM for Chariot assembly. Ultimately, the ITM is designed to be an efficient workspace for in-space assembly and could be effortlessly repurposed for in-space payload assembly for other deep-space missions.

Figure 27: Hooks and footholds in the ITM to aid astronaut assembly of payloads.

5.2.5 Power

Table 30 displays the ITM's electric power subsystem (EPS) requirements to meet the module's power demands for the LEO transit duration.
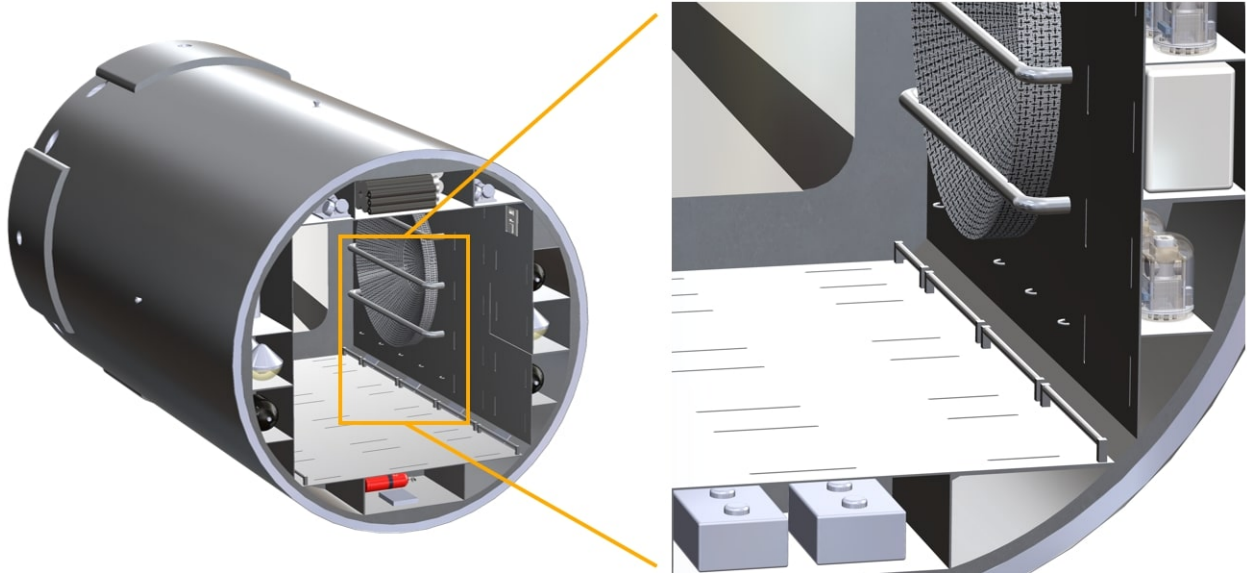
Table 30: Power requirements of the interplanetary transfer module.

ID	Requirement
ITM-POW-01	The ITM's EPS shall provide 1.42 kW of power to its subsystems during orbital maneuvers and docking in LEO.
ITM-POW-02	The ITM's EPS shall provide 385.2 W of power to its subsystems while downlinking during LEO transit.
ITM-POW-03	The ITM's EPS shall provide 152.5 W of power to its subsystems while idle during LEO transit.
ITM-POW-04	The ITM's EPS shall store sufficient energy to power its subsystems for 3 days.

The ITM's EPS is a crucial subsystem to power the module's subsystems during LEO transit to the Deep Space Transport (DST). It was assumed that upon docking with the DST, the ITM would draw power from the DST for the rest of the mission and would no longer need a self-sufficient EPS outside of LEO transit. The ITM's power demands are outlined in Table 31 by subsystem and component.

Table 31: Power budget for the ITM's subsystems during LEO transit.

Subsystem	Peak Power (W)	Downlinking		Maneuvering/Docking		Idle	
		Duty Cycle	Average Power (W)	Duty Cycle	Average Power (W)	Duty Cycle	Average Power (W)
1.0 ADCS/Prop							
1.1 MONARC-445 Thrusters	928	20%	185.6	100%	928	10%	92.8
1.2 MEMS Earth Horizon Sensor	0.15	50%	0.08	100%	0.15	35%	0.05
1.3 Star Trackers	9.9	50%	5.0	100%	9.9	35%	3.5
1.4 HG1930 INS	4	50%	2	100%	4	35%	1.4
1.5 HG1930 IMU	3	50%	1.5	100%	3	0%	0
2.0 Comms/ODH							
2.1 Antennas	5	100%	5	100%	5	10%	0.5
2.2 Processor	5	100%	5	100%	5	100%	5
3.0 TMTC							
3.1 Transponder	26	100%	26	100%	26	10%	2.6
3.2 TWTA	50	100%	50	100%	50	10%	5
Total			280.1		1031.1		110.9
With Contingency (10%)			308.1		1134.2		122.0
Allocated With Margin (25%)			385.2		1417.7		152.5

The EPS design considered the allocated power totals for the subsystem demands, which accounted for a 10% contingency and a 25% margin. During LEO transit, the downlinking and idle power modes are expected to be much more time-dominant over the maneuvering/docking power mode. However, as a contingency plan, the EPS design accounted for the maneuvering/docking power mode being active during 100% of the LEO transit time.

With a total LEO transit time of approximately 2 days, EPS architecture choices were limited to considering a battery-centric architecture. Solar panel-secondary battery or radioisotope thermal generator configurations were determined to be unnecessary for providing the ITM's small power demand over the short time period of LEO transit. Primary batteries were chosen as the ITM's EPS architecture, removing the added mass and volume with a solar panel configuration. After evaluating primary battery specifications by several suppliers, lithium thionyl chloride batteries were chosen for the EPS system for their excellent flight heritage with vehicles like the Philae lander [32] and superior energy densities to other primary battery architectures. Saft, EnerSys, Tadiran, EaglePicher, and Xeno Energy were suppliers investigated for primary battery specifications. In designing the lithium thionyl chloride batteries to meet the ITM's power demands, a mass energy density of 275 W-hr/kg and volumetric energy density of 340 W-hr/dm^3 were used. The results of the battery sizing per battery are displayed in Table 32. As a redundancy measure, the ITM's LEO transit time was assumed to be three days in the event of failed docking sequence(s).

Table 32: Specifications of the lithium thionyl chloride primary batteries.

	Mass (kg)	Volume (m^3)	Energy (kW-hr)
CBE	67.4	0.055	18.6
With Contingency (10%)	74.1	0.06	-
Allocated With Margin (25%)	92.6	0.08	-

For compatibility with the DST's expected bus voltage of 120V, identical to that of the ISS [33] and large spacecraft in flight and in development [34], the circuitry of the ITM will utilize a bus voltage of 120V DC. Subsequently, the batteries for the ITM are intended to be 120V for compatability with the 120V DC bus. To meet the custom demands of the ITM's battery design, EaglePicher was selected as the supplier for the ITM's lithium thionyl chloride batteries for their heritage work and product flexibility. With these voltage and power specifications for the ITM's subsystems in LEO transit, the EPS circuitry wiring is expected to be AWG wire sizes between about 36 AWG and 24 AWG. To meet the low-power demands of the MEMS Earth Horizon Sensor, a 120V DC to 5V DC voltage converter and 36 AWG wire will be used. The wiring sizes were conservatively determined using a rule of 1 amp per 700 circular mils [4]. Importantly, this 120V DC EPS bus will also encompass the ITM's ECLSS and payload deployment subsystems that will draw larger amounts of power from the DST once the ITM is docked with the spacecraft.

Ultimately, the ITM's lithium thionyl chloride primary batteries were placed centrally inside the ITM to minimize wiring to the components. Specifically, the batteries are located in two of the subsystem floor compartments in the ITM. The EPS wiring will primarily run through areas of the module's primary structure, with the propulsion modules and communications equipment demanding the longest amount of

---

[4]https://www.solaris-shop.com/content/American%20Wire%20Gauge%20Conductor%20Size%20Table.pdf

wiring. Fig. 28 provides the battery configuration inside the ITM. For launch, the batteries will be secured to the bottom surfaces of the compartments. The batteries are placed away from sight in the compartments for astronaut convenience, but can be transferred out if the compartment space is needed. Two primary batteries are placed in each of the two power subsystem compartment racks along the floor of the ITM.
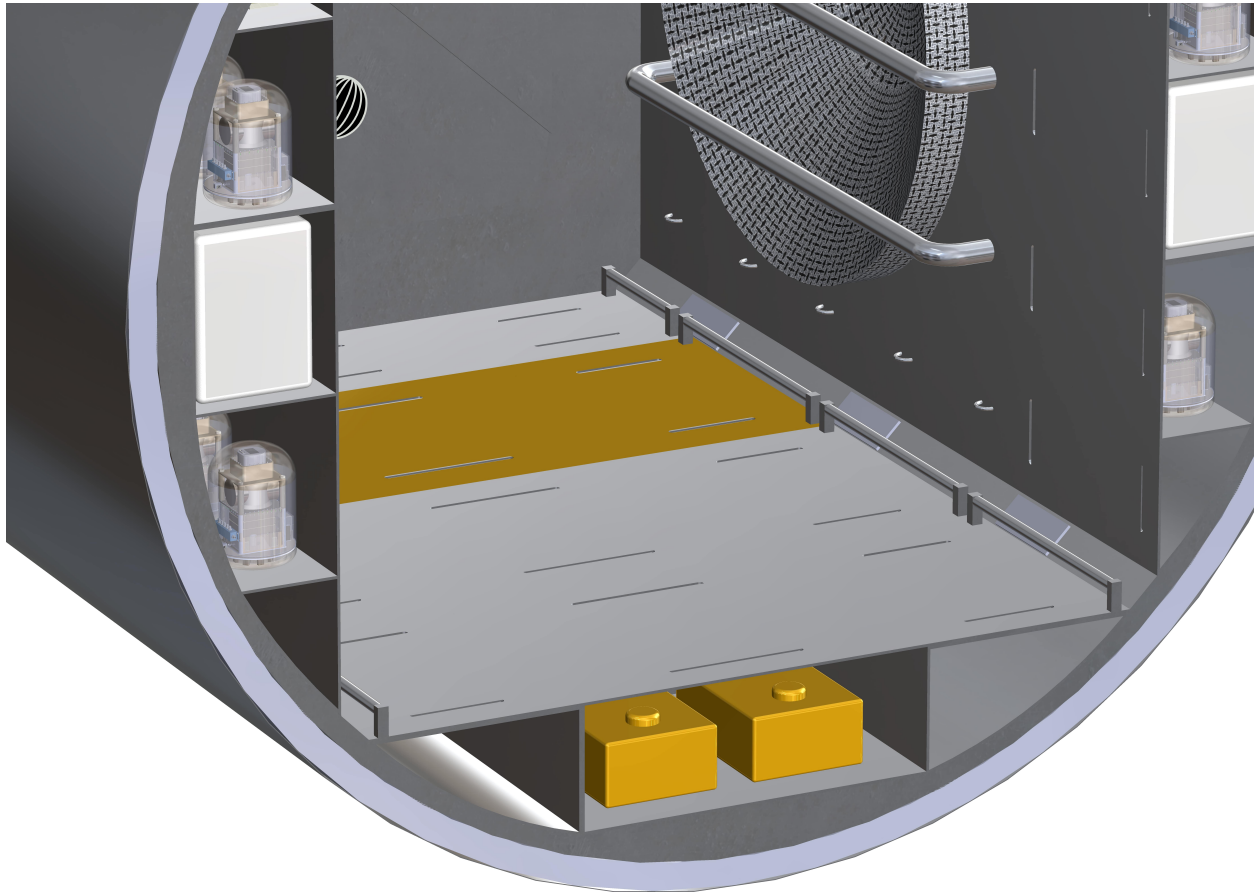

Figure 28: Primary battery configuration inside the ITM, with the visible batteries and second power compartment rack highlighted gold.

5.2.6 Thermal Control System (TCS)

Table 33 shows the ITM's thermal control system (TCS) requirements to regulate the module's internal temperatures during LEO transit.

Table 33: Thermal control system requirements for the interplanetary transfer module.

ID	Requirement
ITM-TCS-01	The ITM's thermal control system shall maintain an internal temperature between $10°C$ and $30°C$ in LEO transit.
ITM-TCS-02	The ITM's thermal control system shall maintain the $10°C$-$30°C$ temperature range for 3 days in LEO transit.

Similar to the ITM's EPS, it was assumed that upon docking with the DST, the ITM would be thermally regulated by the DST's thermal control systems for the rest of the mission and would no longer need a self-sufficient TCS outside of LEO transit. The selected thermal control strategies will act as redundancy measures for the module's thermal regulation once docked with the DST. The ITM's TCS was designed to maintain an internal temperature range between $10°C$ and $30°C$ to lessen the module's initial thermal loads on the DST's TCS. Standard ECLSS temperature ranges for manned spacecraft are $18°C$ to $24°C$ [35]; assuming the DST's TCS regulated the spacecraft's temperature within this range, the ITM's internal temperature range of $10°C$ to $30°C$ was established to keep close to the standard ECLSS range. Additionally, the ITM's internal components are operational within this temperature range.

Preliminary thermal modeling of the ITM utilized a static single node model to assess the ITM's thermal environments during LEO transit and Venus orbit. Additionally, single node analysis calculations were used to establish a thermal control architecture. An illustration of the single node analysis is shown in Fig. 29.
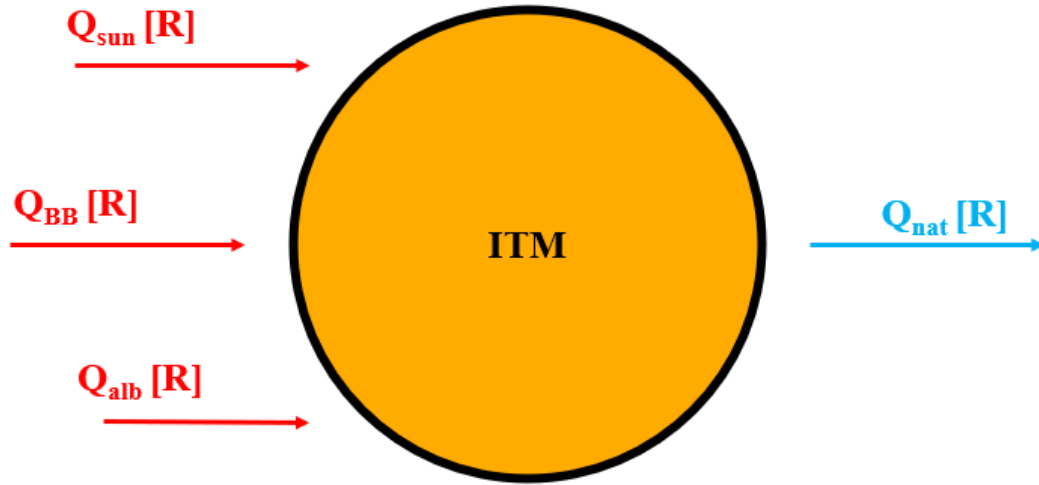

Figure 29: Static single node model representation of the ITM.

Mathematically, the static single node thermal analysis assumes thermal equilibrium and can be represented by the equation

$$Q_{\text{in}} = Q_{\text{out}}, \tag{10}$$

where Q_{in} is the thermal energy input to the system and Q_{out} is the thermal energy output from the system [36]. Expanding the thermal energy terms in Equation (10), the input thermal energy to the ITM comes from solar radiation, blackbody radiation, and albedo radiation. The output thermal energy from the ITM is natural radiation. These radiative thermal energy terms can be expressed using the equations

$$Q_{\text{sun}} = \alpha_{\text{sc}} A_{\text{proj}} S R_{\text{sc}}, \tag{11}$$

$$Q_{\text{BB}} = A_{\text{tot}} F_{\text{sc-p}} \sigma \epsilon_{\text{sc}} (T_{\text{p}}^4 - T_{\text{sc}}^4), \tag{12}$$

$$Q_{\text{alb}} = \alpha_{\text{sc}} A_{\text{tot}} F_{\text{sc-p}} S_{\text{alb}}, \tag{13}$$

$$Q_{\text{nat}} = Q_{\text{sun}} + Q_{\text{BB}} + Q_{\text{alb}}, \tag{14}$$

where Q_{sun} is the thermal energy from the Sun, α_{sc} is the absorptance of the module, A_{proj} is the module's projected area facing the Sun, S is the solar constant 1366.1 W/m^2 at Earth, R_{sc} is the distance of the module from Earth in AU, Q_{BB} is the blackbody radiation thermal energy, A_{tot} is the module's total surface area, $F_{\text{sc-p}}$ is the view factor between the module and the planet [37], σ is the Stefan-Boltzmann constant, ϵ_{sc} is the emissivity of the module, T_{p} is the blackbody temperature of the planet, T_{sc} is the module's temperature, Q_{alb} is the albedo thermal energy, S_{alb} is the planetary albedo constant multiplied by the solar constant at the planet, and Q_{nat} is the module's natural radiative thermal energy. Using these equations, worst-case hot and cold thermal analyses were conducted, with the hot case possessing all radiative thermal energies into the module and the cold case possessing only blackbody radiation. Both cases were calculated for the ITM in Earth orbit for establishing thermal control strategies; in addition, both cases were calculated for the ITM in Venus orbit to find expected thermal loads on the ITM for the DST's TCS. Table 34 shows the results of the single node thermal analyses using an internal module temperature of 20°C.

Table 34: ITM thermal loads with no thermal control strategies.

	Earth	Venus
	Value (kW)	Value (kW)
Hot Case	2.31	13.66
Cold Case	-3.48	-5.76

Thermal control strategies for the ITM's TCS aimed to mitigate the module's radiative heat transfer in LEO and regulate the internal temperature within the established temperature range in Table 33. To reduce TCS complexity and power demands, active thermal control strategies were to only be considered if passive thermal control strategies were insufficient in regulating the ITM's temperature. Multi-layer insulation (MLI) blankets are commonly used on ISS modules [38] and other spacecraft [39] as an effective passive thermal control strategy. Mylar MLI was investigated for the ITM's TCS architecture for its great heritage use [38] [39]; however, Kapton was selected as the primary MLI material for its favorable density of 19 kg/m^3 over Mylar and superior thermal conductance at very low temperatures (4 K) [40] that will be present during interplanetary transit. Specifically, a 30-layer double-aluminized Kapton MLI blanket will be used for the ITM's TCS architecture and will be placed between the outer Aluminum 2024 layer and the Kevlar layer in the ITM's MDPS. A 30-layer blanket was chosen after finding an optimal balance between the MLI's thermal regulation [41], redundant layers for impact resistance within the MDPS, and MDPS mass changes with varying MLI thicknesses. For additional thermal regulation, a thermal coating was required to help establish an equilibrium temperature within the required temperature range in Table 33. Equations (11), (12), (13), and (14) were used to establish a relationship between the ITM's internal equilibrium temperature within the required temperature range and the ratio of absorptivity to emissivity of the module to identify an effective thermal coating. From these calculations, an absorptivity to emissivity ratio between 0.6 and 0.8 was found to appropriately regulate the ITM's internal temperature.

A two-node lumped parameter model analysis was performed to assess the ITM's thermal regulation during LEO transit with the established TCS architecture and refine the absorptivity to emissivity ratio needed for the ITM's thermal coating. This thermal model is illustrated in Fig. 30.
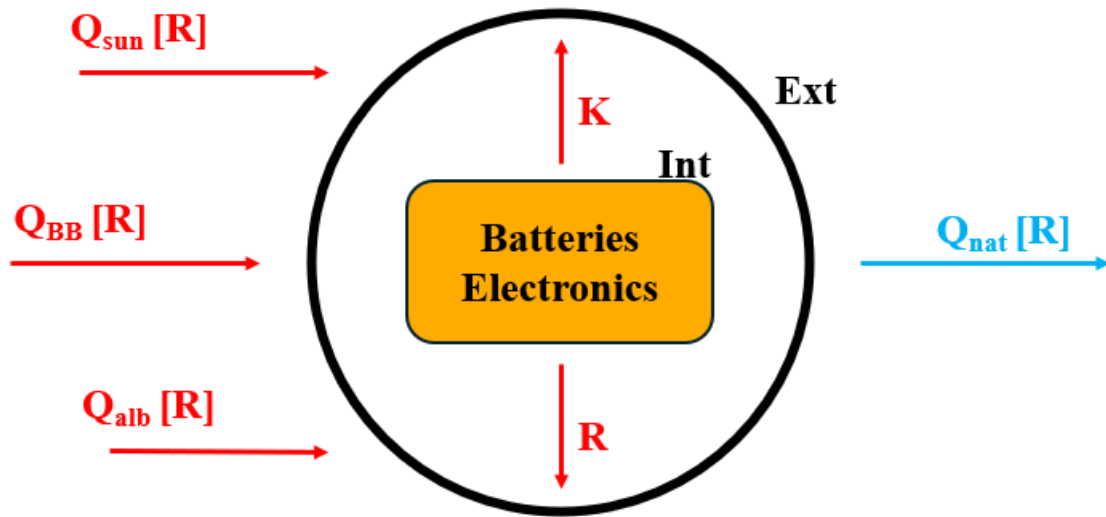
Figure 30: Thermal model representation of the ITM with two nodes: internal and external.

The mathematics behind the ITM's two-node lumped parameter model are derived from a detailed CubeSat two-node lumped parameter model thermal analysis [42]. This CubeSat two-node lumped parameter model, based on a finite element discretization of the body of interest, represents the body as a network of an internal node, an external node, and radiative/conductive links [42]. MATLAB code files associated with the CubeSat thermal analysis were provided, tailored to the ITM and its thermal environment, and subsequently utilized in the ITM's thermal analysis. The module's internal air volume with subsystem components was established as the internal node in the thermal analysis; conversely, the module's primary structure and MDPS configuration was established as the external node in the thermal analysis. This simple yet robust thermal analysis provided temperature-over-time profiles of the ITM in LEO to confirm the effectiveness of the module's TCS. Combining iterative calculations with the lumped parameter model and the calculations with the single node model for the absorptivity to emissivity ratio, the calculated ratio for a $20°$C internal equilibrium temperature was found to be 0.671. Evaluating common thermal control coatings for spacecraft [43] for an absorptivity to emissivity ratio near 0.671, a 0.0001 mils black annodized aluminum coating was chosen as the thermal coating TCS strategy. This coating has an absorptivity of 0.51 and emissivity of 0.75, making the ratio equivalent to 0.68. Results of the lumped parameter thermal analysis with initial cold internal and external temperatures are displayed in Fig. 31. To ensure the module had sufficient thermal regulation over the LEO transit duration, the lumped parameter thermal analysis was conducted over 72 hours.
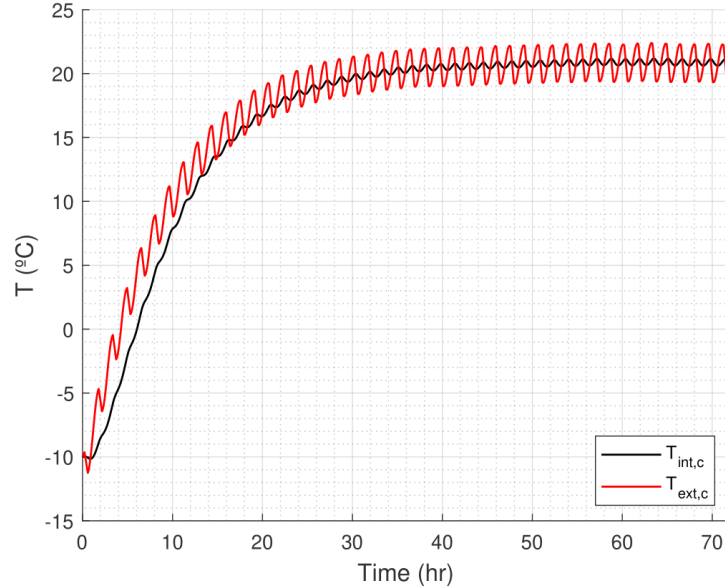
Figure 31: Lumped parameter thermal analysis results with the ITM's TCS and cold initial temperatures.

Results of the lumped parameter thermal analysis with initial hot internal and external temperatures are displayed in Fig. 32. For the cold case, initial temperatures of -10°C were used. For the hot case, initial temperatures of 50°C were used.
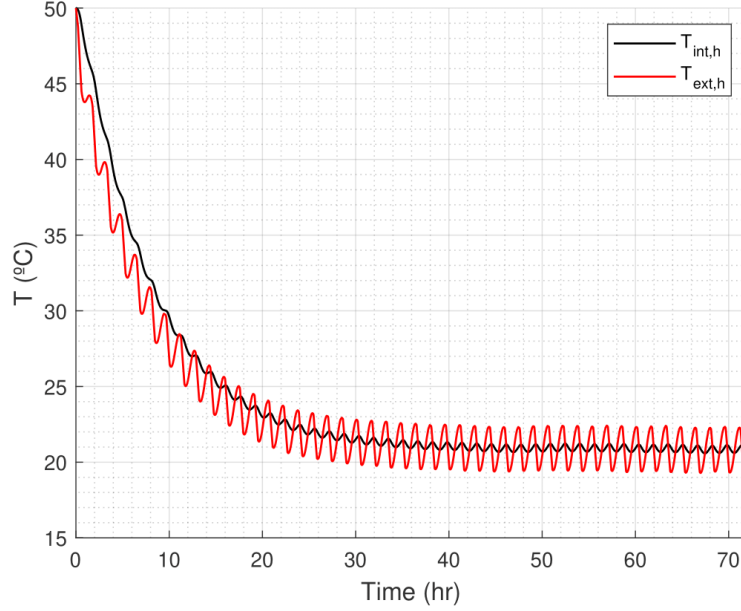
Figure 32: Lumped parameter thermal analysis results with the ITM's TCS and hot initial temperatures.

Ultimately, the results displayed in Figures 31 and 32 show that the ITM's TCS successfully regulates the module's internal temperature and reaches an equilibrium temperature of about 21°C within the LEO transit duration. This equilibrium temperature satisfies the TCS requirements in Table 33. Conducting further lumped parameter thermal analyses with varying initial temperature conditions yield similar results to Figures 31 and 32. The results of the TCS sizing for the MLI blanket are featured in Table 35. Because of the success of the passive thermal control strategies employed on the ITM, no active thermal control strategies are utilized. To provide products and materials for the ITM's TCS, Dunmore was selected as the primary supplier for their wide range of thermal protection products and historical work with NASA.

Table 35: Sizing of the MLI blanket with 10% contingency and 25% margin.

	Mass (kg)	Volume (m^3)
CBE	146.4	1.8
With Contingency (10%)	161.0	2.0
Allocated With Margin (25%)	201.3	2.5

5.2.7 Airlock & Payload Deployment

The airlock is a vital function of the ITM to ensure successful deployment of our payloads in a safe and effective manner. Its configuration is revolutionary as it serves as the first-ever airlock designed exclusively for both large and small payloads. With a volume of 9.26 m^3, the airlock is able to contain and deploy a single Chariot at a time onto Venus. Our airlock is able to depressurize in 3.2 hours when utilizing three Agilent IDP-10 Dry Scroll Pumps, allowing for quick deployment of the Chariots to accomplish our objectives within the 30-day time frame. The key subsystems for the airlock is the air depressurization/pressurization system (ADPS) and the payload deployment system.

5.2.7.1 Air Depressurization/Pressurization System The first mode of the ADPS is the dehumidification of the airlock. In this phase, air is drawn from the airlock and circulated by a fan through a desiccant bed for humidity removal before being returned to the airlock [44]. A fan, desiccant bed, and shut-off valve are all utilized to dry the air in the airlock to a relative humidity less than 30%. The second mode is the depressurization stage where three Agilent IDP-10 Dry Scroll Pumps [45] in series will be used to pump 90% of the airlock air into the ITM to be used for recycling. Three scroll pumps were chosen to ensure redundancy in the design in case of failure of a scroll pump and to increase the pump-down time. The Agilent IDP-10 Dry Scroll Pumps have a base pressure of 1.5×10^{-2} Torr, and the depressurization target for the airlock is 1×10^{-3} Torr. This leads into the third mode of the ADPS which is the vent overboard phase, where valves will be used to vent the remaining 10% of airlock air into space to achieve the depressurization target. After deployment is complete and the external hatch door is shut, the fourth mode of pressurizing the airlock using valves is initiated. Once the pressure inside the airlock is equalized to the pressure of the crewed portion of the ITM, the final regeneration phase begins, where the desiccant bed is reactivated and humidity is restored to the airlock.

Table 36: Specifications of Agilent IDP-10 Dry Scroll Pump.

Specification	Value
Base pressure (60 Hz)	1.5×10^{-2} Torr
Pumping Speed (60 Hz)	10.2 m^3/h at full speed
Volume	0.032 m^3
Motor Rating	350 W
Mass	24.74 kg

The depressurization time can be computed using the following equations [46]

$$t = \frac{V}{S_{\text{eff}}} \ln\left(\frac{P_{\text{i}} - P_{\text{ult}}}{P_{\text{f}} - P_{\text{ult}}}\right), \tag{15}$$

$$p(t) = P_i - P_{ult} e^{-\frac{S_{eff}}{V} t} + P_{ult} \tag{16}$$

where t is time in hours, V is volume of the airlock in m^3, S$_{eff}$ is maximum pump speed, P$_i$ is initial pressure of the system in Torr, P$_f$ is the final targeted pressure in Torr, and P$_{ult}$ is ultimate pressure in Torr of the dry scroll pump. To calculate the depressurization time, the following parameters must be defined.

Table 37: Variables for calculation of depressurization time.

Specification	Value
Volume of Airlock (V)	9.261 m^3
Pump Speed at 100%	15.4 m^3/h
Pump Speed at 75% (S$_{eff}$)	11.55 m^3/h
Initial Pressure (P$_i$)	760 Torr
Final Pressure (P$_f$)	1.5×10^{-2}
Ultimate Pressure (P$_{ult}$)	1×10^{-2}

Using the above equations and specifications listed in the table, for 75% of maximum pump speed and one dry scroll pump, the depressurization time is 9.57 hours. Fig. 33 represents the change in the depressurization time as we increase the number of dry scroll pumps in series.

Overall, the utilization of the Agilent IDP-10 Dry Scroll Pumps prove to be effective in ensuring a robust airlock system, allowing for deployment to occur in a timely fashion.

5.2.7.2 Payload Deployment The payload deployment mechanism is a linear actuator attached to a mechanical slide rail that is based on the JEM slide table in the JAXA Kibo module [19]. The total volume of the mechanical slide rail within the airlock is 0.6 m^3. The deployment of the Chariots and the static drop probes will follow the procedure outlined in the table below.

Table 38: Payload deployment mechanism procedure.

Step	Action
1	Crew sends a command through computer to open internal airlock hatch and extends the Slide Table into the module.
2	Crew secures the Chariots onto the adapter (which already includes the linear release system).
3	Crew moves the Slide Table with the Chariot back into the airlock and closes the hatch.
4	Airlock depressurizes.
5	Crew sends a command to open the external hatch.
6	Slide Table moves the Chariot out of the external hatch.
7	Crew sends a command to deploy the Chariot via linear release mechanism.

When commencing Steps 1 and 3, and 6, the slide rail will move at a speed of 6.7 cm/s such that it will extend to its full length in 30 seconds. The full extension length is 3.2 m to ensure the payloads are deployed
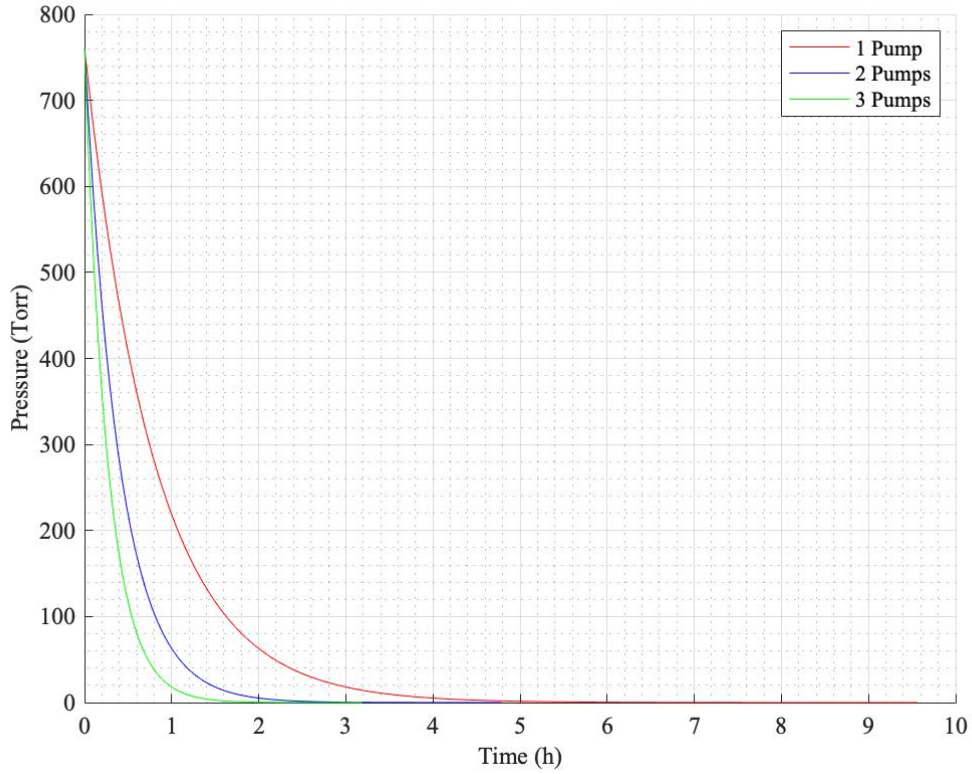
Figure 33: Depressurization time of the airlock depending on the amount of dry scroll pumps.

at a safe distance from the ITM. Once the linear actuator is activated, it will impart a gentle force of 2.85 N on the Chariot or the static drop probe. Once the payload reaches a distance of 10 m from the ITM, approximately at 5.56 minutes, the solid rocket boosters will fire and commence entry into Venus. The CAD models of the deployment mechanism are shown.

5.2.8 Communications and C&DH

There are two main modes for communication that the interplanetary transfer module: communication with the Deep Space Transport and the Deep Space Network. The first main mode for the ITM is to develop a system to transmit and receive information between the ground station and the module itself. Due to distance and data needs, the system uses an S-band patch antenna that spans 1 meter in length and operates at 2 watts. For downlinking mode, the antenna operates at 2425 MHz while the uplink operating frequency is 2050 MHz. Table 39 and 40 provide the calculated link budget for sizing the antenna for the data required for this mode of communication.

The second mode for the ITM is to develop a communication system between the ITM and the Deep Space Transport. The system is necessary to send commands from the ITM to the airlock to enact depressurization
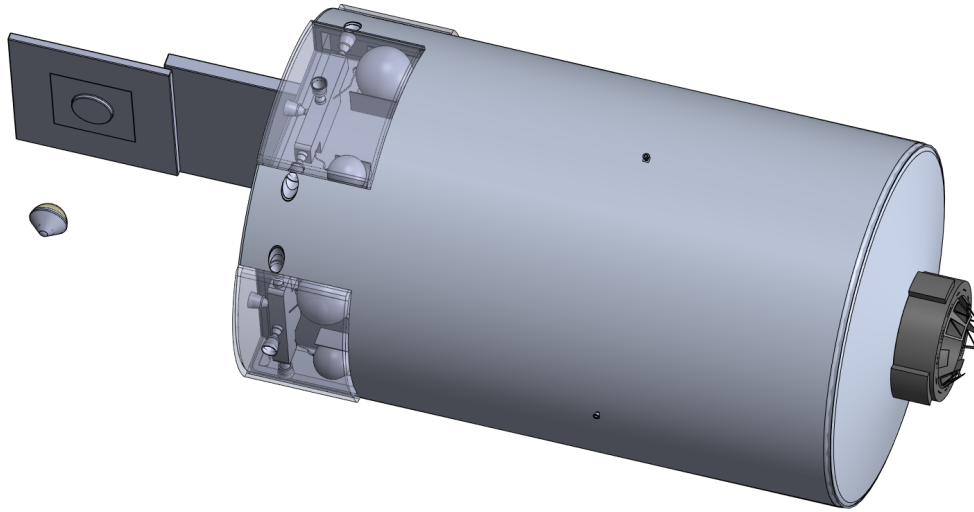
Figure 34: View of the static drop probe being deployed from the linear actuator payload deployment system.

Figure 35: View of the Chariot attached to the linear actuator payload deployment system.

Table 39: Downlink budget for S-band patch antenna for communication with ground station

Downlink Budget: S-Band		
Transmitted Power	4	W
Transmitted Power	6.021	dB
Transmitted Power	36.02	dBm
Transmitter Antenna Gain	8.3	dB
Effective Antenna Gain	7.761	dB
Cable & Beam Loss	-4.9	dB
Path Loss	-131.1	dB
Atmospheric Loss	-0.02	dB
Receiver Power	-112.7	dBm
Receiver Antenna Gain	33.10	dB
CTR	75.70	dBhz
System Noise	-204.3	dBm/hz
Achieved Signal-to-Noise Ratio	14.88	dB
Required Signal-to-Noise Ratio	11	dB
Required Link Margin	**3.880**	

Table 40: Uplink budget for S-band patch antenna for communication with ground station

Uplink Budget: S-Band		
Transmitted Power	1700	W
Transmitted Power	32.30	dB
Transmitted Power	62.30	dBm
Transmitter Antenna Gain	31.64	dB
Effective Antenna Gain	29.59	dB
Cable & Beam Loss	-4.9	dB
Path Loss	-129.7	dB
Atmospheric Loss	-0.02	dB
Receiver Power	-105.7	dBm
Receiver Antenna Gain	-9.94	dB
CTR	77.73	dBhz
System Noise	-204.3	dBm/hz
Achieved Signal-to-Noise Ratio	20.88	dB
Required Signal-to-Noise Ratio	11	dB
Required Link Margin	**9.88**	

and repressurization, open the external hatch door of the module, and receive video feedback from the camera within the airlock itself. Thus, the system uses a VHF turnstile antenna with a maximum RF power of 2 watts. Table 41 provides the calculated link budget for sizing the antenna for the data required for this mode of communication. Since information is only being transmitted a maximum of 1 kilometer, the antenna operates at a downlink frequency of 150 MHz.

Table 41: Downlink budget for VHF turnstile antenna for communication with Deep Space Transport

Link Budget: S-Band		
Transmitted Power	2	W
Transmitted Power	3.010	dB
Transmitted Power	33.01	dBm
Transmitter Antenna Gain	10.45	dB
Effective Antenna Gain	9.771	dB
Cable & Beam Loss	-4.9	dB
Path Loss	-131.1	dB
Atmospheric Loss	-0.02	dB
Receiver Power	-114.6	dBm
Receiver Antenna Gain	33.10	dB
CTR	75.70	dBhz
System Noise	-204.3	dBm/hz
Achieved Signal-to-Noise Ratio	14.02	dB
Required Signal-to-Noise Ratio	11	dB
Required Link Margin	**3.020**	

For both communication systems, an intricate command and data-handling subsystem is necessary for both modes. A SpaceWire data bus is being used for data and system implementation as illustrated in Fig. 36. With increased reliability, this data bus is much newer than the industry standard of MIL-STD 1553 and can handle a maximum throughput of 400 Mbps, an efficiency of 5 bytes overhead without a message size, and can accommodate up to 224 nodes on a single bus. The RAD 6000 CPU with a maximum processing speed of 35 MIPS will execute programs stored in memory, interpret commands, and format data for it to be transmitted to other entities.
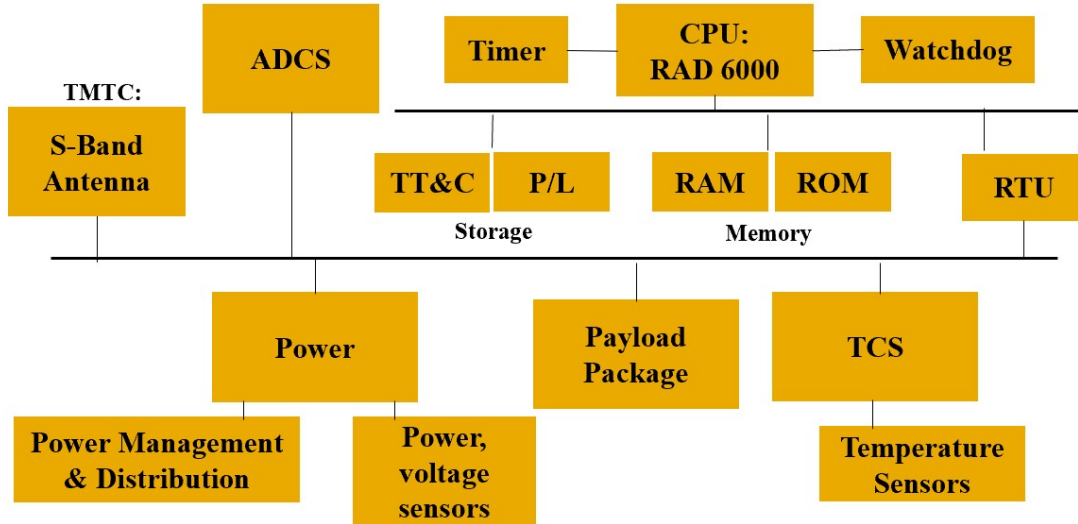

Figure 36: SpaceWire data bus configuration for ITM

6 The Chariot

The Chariot is RHEIA^2's primary mode of mission science gains. Upon completing atmospheric entry, the vehicle will free-fall to 5 kilometers above the Venusian surface, where the pressure is 698 K, the pressure is 6.7 MPa, and the density is 50 kg/m^3. Each chariot has a choice of science packages to conduct lower atmospheric studies, as well as a patch antenna to transmit data to the ITM as it flies overhead. With high-temperature electronics and phase change materials, the Chariot should survive at its operational altitude for 4.1 to 4.2 days.

The ancillary components allowing the Chariot to make atmospheric entry were previously described in the "Chariot Entry, Descent, and Landing (EDL)" and "Chariot Attitude Determination and Control System" sections. The following section will focus on the Chariot's operations after EDL.

Table 42: Chariot requirements.

ID	Requirement
RHEIA^2-CHAR-01	The Chariot vehicle shall retain structural integrity as it descends through the Venusian atmosphere.
RHEIA^2-CHAR-02	The Chariot vehicle shall have the ability to outgas and intake gas so that it can control stresses during descent.
RHEIA^2-CHAR-03	The Chariot vehicle shall float at an altitude of 5 km above the surface of Venus utilizing a mixture of water vapor, helium gas, and intake air.
RHEIA^2-CHAR-04	The Chariot shall carry a scientific payload, utilize it in study of Venus, and transmit data back to the ITM in orbit.

6.1 Chariot Trade Studies

The use of a balloon to observe Venus is not without precedent, as seen in the Soviet Vega missions[47] and the conceptual designs proposed by Geoffrey Landis in his paper on the subject [4]. Landis notes that the Vega missions took place only in the "relatively benign" [4] upper atmosphere, where heat and pressure are not as significant as the lower atmosphere, and took place on the dark side of Venus to avoid the need for extreme thermal protections. The high-altitude exploration of the Vega missions poses a different set of challenges when compared to Landis' low-altitude proposal and the Chariot plan. The use of a metal shell came about due to an increase in atmospheric density, meaning the balloon could be more dense, as well as an increase in temperature and pressure, meaning the balloon had to be strong enough to resist those conditions. Landis' article served as a technical sizing basis for the Chariots, but further calculations caused our design to differ from the original proposed figures, primarily due to a need for a thicker shell to survive the predicted pressure differentials.

6.2 Chariot Structure

The Chariot's load-bearing structure is modeled as a uniform metal sphere made from Ti-6Al-2Sn-2Zr-2Mo-2Cr-0.25Si, hereinafter referred to as "titanium alloy." The shell is 1.621 meters in diameter and 1.652 millimeters thick. In reality, the shell also implements two O-rings and fasteners to attach the two halves together. The shells were sized with the primary considerations of keeping the overall vehicle at 50 kg/m^3 and surviving the pressure differentials of the descent into Venus' lower atmosphere.

Table 43: Chariot Shell Properties.

Parameter	Value	Unit
Diameter	1.621	m
Thickness	1.652	mm
Internal Volume	2.2166	m^3
Helium stored	0.8455	kg
Water stored	30.4431	kg
Maximum experienced pressure differential	2.1809	MPa
Material	Ti-6Al-2Sn-2Zr-2Mo-2Cr-0.25Si ss	
Modulus of Elasticity	1.23*10^{11}	Pa
Ultimate Tensile Strength	1.070*10^9	Pa

In order to save space, the Chariot is transported to Venus in parts: two large hemispherical halves, the payload bays, the antenna, the heat shields, the boosters, the o-rings, and the fixtures needed to attach the pieces together (screws, some wire for the antenna).

Notably, the hemisphere halves are not identical: one half, the bottom, will have a hole on the bottom so that the instruments can be properly exposed to the Venus atmosphere, and will also have mounting points for the boosters. In contrast, the top hAlrigalf will have fixtures to allow the wiring through and holes for the intake and outtake valves required. Both halves will also have holes to allow for the screws to connect the two halves, and one of the halves will have a 'lip' that overlaps with the other half so the screws actually connect the two portions of the Chariot. Threading built into the inner hemisphere will give the screw something to attach to, and high-performance thread sealant will control leakage around the screws. Leakage near the connection of the two halves will also be controlled by a large, custom-made O-ring inserted in the overlapping region, where it is pressed between the two halves by the force of screws.

6.2.1 Structure Requirements

6.2.2 Structure Trade Studies

As designed, there are no internal supports inside, unlike the structure proposed in the Landis paper [4]. A more advanced shell design with internal bracing may be able to reduce system weight further. Such

Table 44: Chariot structural requirements.

ID	Requirement
CHAR-STR-01	The structure shall carry the Chariot's scientific instruments and power systems within itself to protect them during descent.
CHAR-STR-02	The structure shall be assembled by a crew of four in the ITM using only hand tools that cause no sparks.
CHAR-STR-03	The structure's burst pressure shall be at least twice the expected pressure encountered during descent.
CHAR-STR-04	The structure shall store lifting fluid in both liquid and gas form through both positive and negative outside pressure differential, depending on operational state.
CHAR-STR-05	The structure shall be made from a material which is able to be shaped into a sphere and has been used in previous aerospace or other structural applications.

weight savings could go to implementing the O-rings, if the calculated shell including them ends up being heavier, or reducing the size of the Chariot design. A few holes in the shell must be installed: one at the bottom, in order to allow the scientific payload proper access to the atmosphere and two to allow for intake and outgassing valves.

For structural simplicity and with Finite Element Analysis (FEA) being out of the scope of the project's time frame, the structure was treated as a uniform titanium shell designed to withstand twice its expected encountered pressure.

Table 45: Shell Sizing Variable Definitions

Variable	Definition	Units
h	Height	km
T	Temperature	K
ρ	Density	kg/m^3
R	Universal gas constant	J/K*mol
n	Number of moles	mol
P	Pressure	Pa
r_{Bal}	Chariot Radius	m
p_b	Burst Pressure	
o_a	Allowable tensile ultimate stress	N/m^2

To compute the shell's dimensions, the group used a MATLAB script which modeled the ambient pressures and temperatures of Venus up to 43 kilometers above the surface, using two polynomial equations 17 and 18 [48] and calculating pressure by the ideal gas law in equation 19.

$$T = -5 \cdot 10^{-6} \cdot h^4 + 0.0014 \cdot h^3 - 0.0865 \cdot h^2 + -6.4443. \cdot h + 732.47 \tag{17}$$

$$\rho = -7 \cdot 10^{-9} \cdot h.^5 + 3 \cdot 10^{-6} \cdot h^4 + -0.0007 \cdot h^3 + 0.0677 \cdot h^2 + -3.3302. \cdot h + 64.87 \tag{18}$$

$$pv = nRT \tag{19}$$
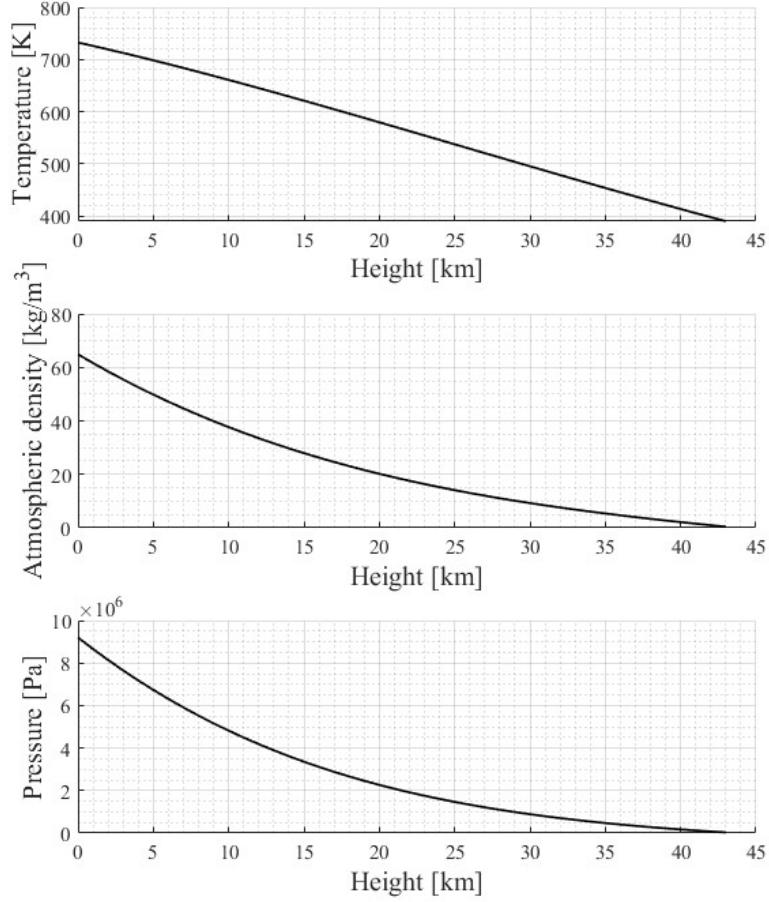
Figure 37: Venus atmospheric parameters over height calculated by polynomial equations.

The balloon, in turn, had its own internal pressure, whose main contributors are the internally stored Helium and water vapor. The helium is modeled by the ideal gas law.

The water, due to its non-ideal behavior, is modeled by the Antoine equation [49]. Pressure "P" is expressed as Bar in this equation.

$$\log_{10}(P) = A - (B/(T + C)) \tag{20}$$

The shell, in turn, is computed as a spherical pressure vessel whose burst pressure is twice the expected pressure.

Table 46: Antoine Equation Parameters for Water.

$256 < T < 373$	Definition
A	4.6543
B	1435.264
C	-64.848
T > 373	**Definition**
A	3.55959
B	643.748
C	-198.043

$$t_{\text{ShellReq}} = P_b \cdot r_{\text{Bal}}/(2\sigma_a) \tag{21}$$

6.2.3 Chariot Iterative sizing process

Initially, the required shell thickness ranged from 2 to 6 times what was necessary to keep a Chariot at a 5 km altitude. Thus, the Chariot architecture underwent several optimizations:

- The optimizations were primarily based around the peak pressure differentials the Chariot experienced during descent: a peak outwards pressure around 30 km and a peak inwards pressure at 5 km, the operational altitude.

- Instead of completely negating pressure at 5 km, the internal gases were re-calculated to operate at approximately 5 bar at that altitude. This pressure was lower than the approximate 6.8 bar at 5 km, but the shell would be designed to survive that pressure differential.

- At the same time, the lowering of operational internal pressure would lower the internal pressure across the board, alleviating the peak outwards pressure.

- To maximize structural efficiency, the internal gas concentrations were adjusted so that the maximum outwards and inwards pressure differentials were identical, meaning the shell would have the same required thickness for the two cases.

A manual iteration process shifted the design point to its final optimized state, with a few guidelines for iteration being listed below:

- A larger shell holds more gas and lowers overall density, but is harder to store in the ITM. A shell larger than approximately 2 meters would be impossible to take out of the airlock.

- The shell is exactly as thick as required to withstand twice the expected pressure for contingencies.

- Outgassing more during the high-altitude phase alleviates high altitude pressure differential but will require more CO_2 intake at low altitude.

- Both outgassing and some level of shell thickness are required to make the design viable. However, both increase mass. At some points, increasing shell thickness and lowering outgassing percentage will lower the overall operational system mass, and vice versa.

- The above back-and-forth exchange between outgassing and shell thickness was performed until a minimum operational density was reached, at which point the shell diameter was increased. This process repeated, with the shell being enlarged again if needed, until the final design point was reached.

Table 47: Design points over iterations, with final design point at bottom.

Diameter (m)	Thickness (mm)	% Outgas	Operating Pressure (MPa)	Density Initial	Density Final
2	1	0.5	5	32.7403	49.4543
1.7	1.6504	0.85	5	48.7298	49.6598
1.65	1.7	0.9	5.04	51.2007	49.7995
1.6	1.5578	.87	5.08	50.5451	50.4177
1.6	1.55	.867	5.08	50.4101	50.4309
1.6	1.56	.8705	5.081	50.586	50.4181
1.6	1.6359	.9	5.05	51.8141	50.412
1.621	1.652	.901	5.05	51.3727	49.9989

With the final design point, figure 38 illustrates the pressure differentials experienced by the Chariot across its heights of operation. The mission timeline goes right to left as the balloon descends.

6.3   Chariot Science Payloads

For ease of in space manufacturing, the scientific payloads were designed to be modular. This resulted in several scientific payload packages, or instrument suites, being developed. Each package was assembled with some key ideas in mind: 1) A general common science goal should be investigated, 2) The relative sizing of such instruments should be able to fit inside the structure of the architecture, 3) The packages should act like a diverse tool kit for the human crew. Due to the modular nature of the payload packages there are nearly endless possibilities of what science can be conducted with the only constraints being the physical operating environment/altitude of the Chariot. The same study conducted by NASA's JPL Venus Aerial Platforms Study Team identified several instruments best for aerial application based on scientific objectives [50].
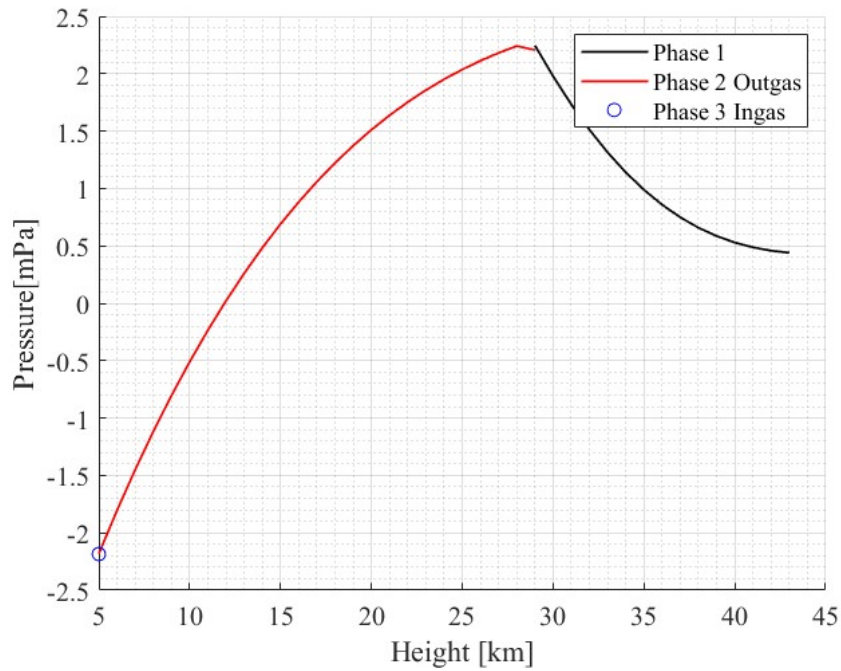
Figure 38: Chariot pressure differentials across phases of flight.

Table 48: Scientific Instruments identified as candidates for deployment on the aerial platform from JPL's Venus Aerial Platforms Study Team

Instruments	Measurement Type/Objectives
Atmospheric Gas Composition	
Mass Spectrometer	Atmospheric species including noble gases and their isotopes. Survey instrument
Tunable Diode Laser Spectrometer	Trace species including isotopic abundances. Targeted on a few species
UV/IR Spectrometer	Atmospheric species from their spectal signatures. Survey instrument
Chemical Sensors (MEMS based)	Chemical species. Small low power instrument targeted on a few species
Cloud and Haze Particles	
Nephelometer	Size, scattering properties and abundance of cloud and haze particles in bulk
Light Optical Amospheric Counter	Size, scattering properties and abundance of cloud and haze particles individual
Imaging Microscope	Images larger cloud particles captured on a filter.
Aerosol Mass Spectrometer	Chemical composition or biological nature of aerosols (individual or bulk)
Atmospheric Structure	
Atmospheric Structure Instrument	Temperature, pressure and vertical wind speed.
Net Flux Radiometer	Upward and downward flux of radiation in multiple spectral bands
Ultra Stable Oscillator	Wind velocity from Doppler signatures from DSN and orbit
Lightning Detector	Transient EM, optical and acoustic signals indicative of lightning
Geophysical Sensors	
Magnetometer	Remanent magnetic fields indicative of early Venus dynamo
Electromagnetic Sounder	Crustal thickness and conductivity
Gravimeter or Gradiometer	Gravity anomalies at high resolution
Infrasound Sensor	Infrasound from Venus quakes and volcanoes
Surface Observations	
NIR Imager	Thermal emission from the surface viewed from below base of clouds
Visible Imager	Surface imaging at high resolution (sub-meter). Probe or sonde instrument

By pairing the Chariot's science objectives with Table 48 several payload packages can be developed.

6.3.1 Payload Packages

Based on the Chariot's science objectives, currently RHEIA^2 has developed 3 payload packages for the Chariot. Each of the packages will contain three supporting instruments along with a primary instrument. The primary instrument is placed at the large bottom port of the package in order to access the Venus environment to collect its data.

Table 49: Chariot Science Payloads

Package	Instrument	Science Objectives
All	IMU (Inertial Measuring Unit)	- Wind Characterization - Global Circulation - Vertical Motions
	Oxygen Detector	- Atmospheric Characterization - Biologically Relevant Chemistry
	Temperature & Pressure Sensor	- Atmospheric Characterization - Radiative Balance
Persephone	Visible Imager	- Characterize Differentiation - Geophysical Studies - Rock Weathering Investigations
Charon	NIR Imager	- Geophysical Studies - Rock Weathering Investigations
Zephyrus	Net Flux Radiometer	- Greenhouse/Cloud Physics - Active Volcanism & Tectonism

Future payload packages could address very different science objectives such as Differentiation. This could be done by developing concepts such as a Venus aerial seismometer [51]. Another potential payload package could contain a gravimeter and barometer in order to detect gravitational anomalies on the Venusian surface. The ability to measuring gravity close to the surface would provide great data for studying volcanoes, coronae, and others.

6.4 Chariot Power

6.4.1 Chariot Power Requirements

6.4.2 Power Subsystem Selection

Based on available research and a contemporary understanding of Venus surface conditions, the RHEIA^2 low atmosphere Chariots will be powered by a singular secondary battery with no recharging capabilities.
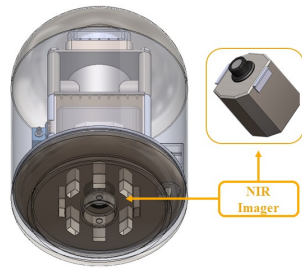
(a) Charon
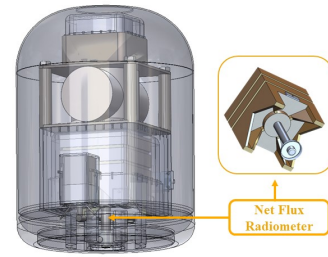
(b) Zephyrus
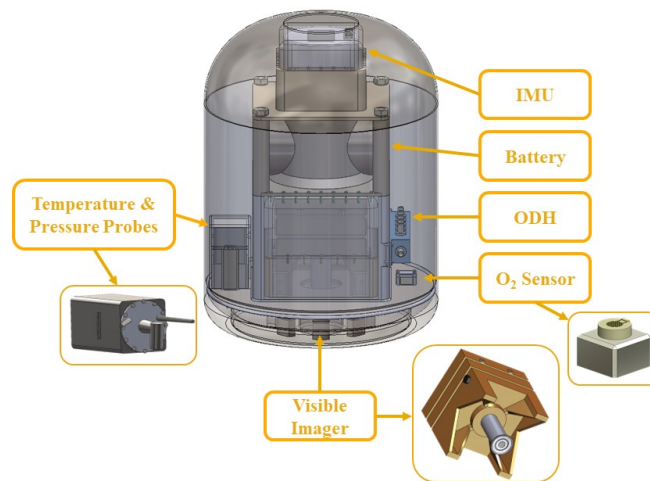
(c) Persephone

Figure 39: Configuration of Payload Bays

Table 50: Chariot power requirements.

ID	Requirement
CHAR-POW-01	Adequate power shall be provided to the pertinent subsystems while in operation.
CHAR-POW-02	Power drain shall be minimized while maintaining sufficient science return.
CHAR-POW-03	The power subsystem shall have an operating temperature near Venus ambient temperatures at operational altitudes.
CHAR-POW-04	The power system shall operate through the lifetime of the Chariot's operation with no recharging capabilities.

The iron sulfide cathode battery was selected for its high operating temperature, which extends beyond Venus surface temperatures, high theoretical energy density, "excellent thermal stability, high utilization discharge rates [and] good electrochemical reversibility" [52]. This battery chemistry has also shown promising results in initial single cell testing [52] as well as in more advanced 17-cell designs [53] which more closely match with what would be needed in the RHEIA^2 low altitude Chariots.

6.4.3   Analysis of Other Architectures

Solar panels were ruled out early on in the design as a method of power generation. Power generation from solar panels at the surface of Venus is estimated to be between $2W/m^2$ and $8.7W/m^2$ at the surface and $22W/m^2$ at an altitude of 5 km [52, 54]. These values are too low to be considered a viable option within the mass budget. Radioisotope Thermoelectric Generators (RTGs) are similarly unreasonable because of our mass budget, but additionally, there are significant cooling issues with RTGs, which have not been explored at ambient Venus temperatures.

This leaves the selection of a primary or promising secondary battery which will power the balloon for the duration of its mission with no recharging capabilities. Because of the these limitations, as well as environmental conditions, the selected battery chemistry must have a high energy density, low discharge rate over the course of about 7 days, and an operating temperature near or above Venus surface conditions. Typical lithium ion batteries have operating temperatures far below low altitude atmospheric temperatures on Venus, typically around $100°C$, which is unrealistic for the thermal control of the Chariot. Additionally, typical molten salt batteries have operating temperatures around $350°C$, but there are no studies demonstrating their viability beyond $400°C$, and initial analysis shows the cathode in typical molten salt batteries will begin to decompose well below Venus surface temperatures [52].

6.4.4 FeS Cathode Battery Specifications

Table 51: Theoretical values for FeS performance

Specific Capacity (mAh/g) [52]	Specific Energy (Wh/kg) [52]	Volumetric Capacity (mAh/cm^3) [55]	Battery Density (L/kg)
610	1036	2950	0.207

Table 52: Known values for FeS battery performance

Operating Temperature ($°C$) [52]	Operating Pressure
up to 475	unknown

Table 53: FeS battery specifications for use in the RHEIA^2 balloon system

Component	Mass (Kg)	Available Energy (kWh)	Available Capacity (Ah)	Volume (L)
Battery	4.0	2.6	1580	$\sim$
Pressure Vessel	0.239	$\sim$	$\sim$	0.92

Due to the low TRL of the battery at present, a 35% contingency will be be applied to the values in Table 1. Table 3 shows the battery specifications based on the mass budget and the contingency described above.

Payload Package Power Budgets

Table 54: Persephone Package Power Budgets

Persephone				Descent		Science	
Subsystem	Component	Peak Power (W)	Duty Cycle (%)	Average Power (W)	Duty Cycle (%)	Average Power (W)
1 - Comms							
	1.1 UHF	2	100%	2	100%	2
	1.2 Patch	4	100%	4	100%	4
2 - Payloads							
	2.1 - NIR Imager	50	0%	0	5%	2.5
	2.2 - Temperature Sensor	0	0%	0	100%	0
	2.3 - Pressure Sensor	1.5	0%	0	100%	1.5
	2.4 - Oxygen Detector	5	0%	0	75%	3.75
	2.5 - IMU	12	0%	0	100%	12
3 - ADCS							
	3.1 - Reaction Wheel Config.	32	50%	16	0%	0
	Totals			22		25.75

Table 55: Charon Package Power Budgets

Charon				Descent		Science	
Subsystem	Component	Peak Power (W)	Duty Cycle (%)	Average Power (W)	Duty Cycle (%)	Average Power (W)
1 - Comms							
	1.1 UHF	2	100%	2	100%	2
	1.2 Patch	4	100%	4	100%	4
2 - Payloads							
	2.1 - NIR Imager	4	0%	0	75%	3
	2.2 - Temperature Sensor	0	0%	0	100%	0
	2.3 - Pressure Sensor	1.5	0%	0	100%	1.5
	2.4 - Oxygen Detector	5	0%	0	75%	3.75
	2.5 - IMU	12	0%	0	100%	12
3 - ADCS							
	3.1 - Reaction Wheel Config.	32	50%	16	0%	0
	Totals			22		26.25

Table 56: Zephyrus Package Power Budgets

Zephyrus				Descent		Science	
Subsystem	Component	Peak Power (W)	Duty Cycle (%)	Average Power (W)	Duty Cycle (%)	Average Power (W)
1 - Comms							
	1.1 UHF	2	100%	2	100%	2
	1.2 Patch	4	100%	4	100%	4
2 - Payloads							
	2.1 - Net Flux Radiometer	10	0%	0	25%	2.5
	2.2 - Temperature Sensor	0	0%	0	100%	0
	2.3 - Pressure Sensor	1.5	0%	0	100%	1.5
	2.4 - Oxygen Detector	5	0%	0	75%	3.75
	2.5 - IMU	12	0%	0	100%	12
3 - ADCS							
	3.1 - Reaction Wheel Config.	32	50%	16	0%	0
	Totals			22		25.75

Regarding the lifetime of the battery, considerations must be made of the duration that the Chariot will operate in each power mode. The descent power mode is assumed to last for one hour, and the science mode is assumed to last from that point onward with no planned standby. Based on a total of 2.6kWh available, the projected battery lifetimes are shown below.

Table 57: Battery Lifetime Estimates

Payload Package	Lifetime Estimate (days)
Persephone	4.19
Charon	4.11
Zephyrus	4.19

6.5 Chariot Thermal Control

The thermal control subsystem, constructed as a passive and modular system, is tailored to meet diverse requirements stemming from the four distinct payload packages. A passive system was chosen because of the its low cost, low weight, and operational simplicity. The modularity is achieved through the creation of thermal boxes designed to seamlessly adapt to the assorted dimensions of payload packages, a range of operating temperatures, and the specific instrumentation needs for atmospheric exposure, visual access to the atmosphere, or complete isolation. These thermal boxes consist of 20 layers of embossed double aluminized Kapton, a multi-layer insulation material, enveloping the outer layer of the box, and of sodium nitrate, a

phase changing material, enveloping the payloads. Another component of the thermal control subsystem is an ablative heat shield, designed to assist in thermal protection during EDL.

6.5.1 Thermal Boxes

The thermal boxes, of dimensions 40cm x 12.5cm x 12.5cm, consist of two sides: side A and side B. Side A will contain payload instrumentation that have higher operating temperature ranges, and that require atmospheric exposure. Side B will contain instrumentation that have lower operating temperature ranges and that either require visual access to the atmosphere or no access at all. This design choice was made to cluster instruments with comparable operating temperature ranges and atmospheric needs in order to prevent thermally sensitive instruments from reaching their maximum lifespan prematurely.

6.5.2 Multi-Layer Insulation

Multi-layer insulation blankets were selected for their effectiveness in mitigating excessive heat absorption from the environment and preventing heat loss from components. Comprising 20 layers of low-emittance films, these blankets offer radiation protection specifically during entry, as radiation becomes significant only in the upper atmosphere, with the sulfuric acid cloud layers substantially diminishing radiation at the surface. Embossed double aluminized Kapton was chosen as the multi-layer insulation material because of its low mass and thermal properties. The selection of this material is also attributed to its suitability for high-temperature applications, exemplified by its utilization in the Cassini program [56].

A general criterion for interior blanket layers is the need for low emittance. As indicated in table 58, aluminized Kapton exhibits an emittance value of 0.03. The embossed patterns serve as low-conductive spacers, creating separation between blanket layers. The decision to employ 20 layers represents a balance between allocated mass and thermal protection: increasing mass would lower the operational altitude and pose more challenges in maintaining the instrumentation's cool temperatures. The properties of double aluminized Kapton are shown in table 58 [56].

6.5.3 Phase Changing Materials

Phase changing materials were selected for two primary reasons: their proven reliability in aerospace projects for maintaining electronic components at precise temperatures and their capability to absorb the power dissipated by these electronic components [56]. Sodium nitrate was selected due to its low thermal conductivity and suitability for high-temperature applications. It stands out among phase changing materials as one of the few options with a temperature range between 578-778 Kelvin, featuring a melting point at 584

Kelvin [57]. Furthermore, its noteworthy high latent heat of fusion (174.13 J/g) ensures a prolonged period for phase change. More thermal properties of Sodium Nitrate can be seen in table 58.

Table 58: Material properties of Thermal Control subsystem

Potassium Nitrate			
Density (g/cm^3)	Melting Temperature (K)	Latent Heat of Fusion (J/g)	Thermal Conductivity (W/mK)
2.26	584	174.13	0.62
Double Aluminized Kapton			
Thickness (mm)	Weight (gm/cm^2)	Abosrptance	Emittance
0.127	0.019	0.12	0.03

6.5.4 Thermal Analysis

The result of the Lumped Parameter Thermal Analysis can be seen in table 59. This analysis, done through MATLAB, incorporates the thermal properties and dimensions of the titanium shell (chosen for its advantageous thermal characteristics), the Multi-Layer Insulation, and the Phase Changing Materials. Critical assumptions considered include the complete ablation of the heat shield and the absence of heat transfer onto the balloon throughout EDL, which include the thermal effects of pyrolysis. In order to model the atmosphere, temperature [17] and density curve fits were used, which were derived from NASA's Venus-GRAM [58]. While the temperature curve fit seemed accurate at any altitude, the density curve only seemed accurate near the surface. Therefore, we incorporated an exponential density model [22] using the planet's scale height and the density at the surface.

$$\rho = \rho_0 e^{-h/H} \tag{22}$$

Upon comparing the exponential density model with the curve fit model, we observed agreement in data up to an altitude of 27 km. Beyond this point, we opted to exclusively use the exponential density model, considering it more precise. It is important to note that this model does not account for the abrupt density changes within the sulfuric acid cloud layer. The data in table 59 corresponds to the point at which the Phase Changing Materials reach complete melting. Certain instrumentation with high operating temperatures will continue to operate even after the Phase Changing Materials melt.

Note: the Power and Communications subsystems chose materials such that the they can operate at Venus ambient temperature without Thermal Control.
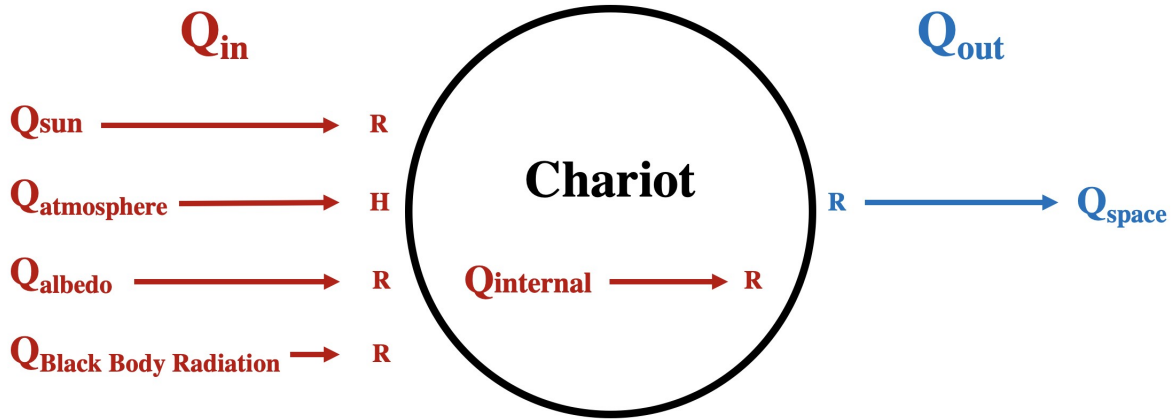
Figure 40: Single node thermal analysis

Table 59: Thermal analysis results

Altitude (km)	Lifetime (days)
5	4.1

6.6 Chariot Communication and C&DH

Serving as a low-altitude balloon, the chariot is a modular design that has three main payload packages: the Persephone suite, the Zephyrus suite, and the Charon suite. Each suite focuses on a different part of the scientific study depending on what suite the humans choose for the mission. Table 60 shows in more detail the data requirement for each payload package.

Table 60: Data budget for three potential payload packages for the Chariot

Payload Package	Data (bps)	Contingency (15%)	Total (Kbps)
Persephone			8823
Visible Imager	5900000	6785000	
Temperature Sensor	1000	1150	
Pressure Sensor	500	575	
Oxygen Detector	10	11.5	
Accelerometer + Gyro	800	920	
Zephyrus			4.649
Temperature Sensor	1000	1150	
Pressure Sensor	500	575	
Net Flux Radiometer	800	920	
Accelerometer + Gyro	800	920	
Oxygen Detector	10	11.5	
Charon			3.752
NIR Imager	200	230	
Pressure Sensor	500	575	
Temperature Sensor	1000	1150	
Oxygen Detector	10	11.5	
Accelerometer + Gyro	800	920	

With each package having various requirements, two antennas are utilized to transmit data from the chariot to the ITM. The first antenna on the Chariot is the X-band patch antenna. Operating at 8350 MHz, the antenna sends signals to ITM at a bit rate of 43 Mbps. The X-band antenna will be responsible for all main science data collected and sent by each chariot. Table 61 shows the downlink budget for the patch antenna.

Table 61: Downlink budget for X-band patch antenna

Link Budget: X-Band		
Transmitted Power	2	W
Transmitted Power	3.010	dB
Transmitted Power	33.01	dBm
Transmitter Antenna Gain	2.256	dB
Effective Antenna Gain	2.112	dB
Cable & Beam Loss	-4.9	dB
Path Loss	-104.9	dB
Atmospheric Loss	-0.02	dB
Receiver Power	-112.9	dBm
Receiver Antenna Gain	16.61	dB
CTR	76.26	dBhz
System Noise	-204.3	dBm/hz
Achieved Signal-to-Noise Ratio	15.03	dB
Required Signal-to-Noise Ratio	11	dB
Required Link Margin	**4.03**	

For redundancy, an additional antenna is attached to the chariot. The UHF patch antenna operates at 450 MHz and transmits science data to the interplanetary transfer module, as seen in Table 62 detailing the downlink budget required for this mode of communication.

Table 62: Downlink budget for UHF patch antenna

Link Budget: UHF		
Transmitted Power	5	W
Transmitted Power	6.989	dB
Transmitted Power	36.99	dBm
Transmitter Antenna Gain	-15.11	dB
Effective Antenna Gain	-14.13	dB
Cable & Beam Loss	-4.9	dB
Path Loss	-79.48	dB
Atmospheric Loss	-0.02	dB
Receiver Power	-113.3	dBm
Receiver Antenna Gain	4.311	dB
CTR	76.26	dBhz
System Noise	-204.3	dBm/hz
Achieved Signal-to-Noise Ratio	14.71	dB
Required Signal-to-Noise Ratio	11	dB
Required Link Margin	**3.71**	

With a lifetime of four days, implementing sufficient command and data handling systems that can handle at minimum 37 Mbps is crucial to the success of the mission. In order to provide the humans science data from each instrument package, a MIL-STD-1773 data bus with a 1 Mbps data throughput is essential to mission success. The bus, illustrated in Fig. 41, requires minimal power but serves as the most reliable system for data transmission of multiple processing units. Along with the data bus, a RAD 3000 CPU will be integrated into the system. With 16 MB RAM and a maximum 10 MIPS sizing, this computer processing unit should be able to handle the processing of data throughout the mission, especially since the CPU is RAD hard which is ideal for the Venusian corrosive environment
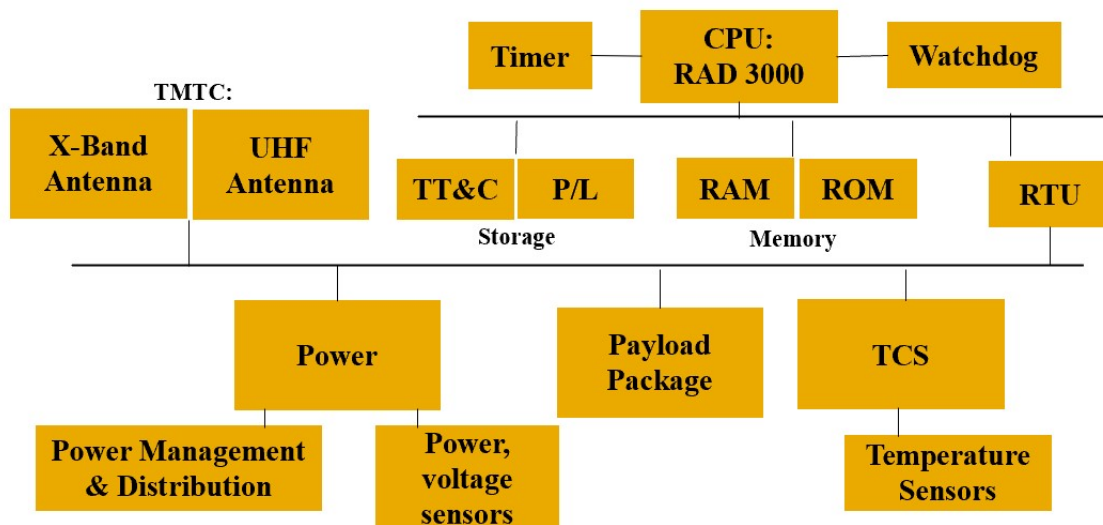
Figure 41: MIL-STD-1773 data bus configuration

7 The Static Drop

7.1 Static Drop Requirements

ID	Requirement
SD-01	The Static Drop shall deorbit and enter the Venusian atmosphere while keeping its payload intact.
SD-02	The Static Drop shall transmit scientific data from Venus until it crashes.
SD-03	The probe shall ensure that all sensors, including visual ones, can observe Venus.

7.2 Static Drop Trade Studies

An additional scientific goal we wanted to accomplish was upper atmosphere characterization, and for that purpose, we have the Static Drop. Its design takes inspiration from another plan for a relatively small Venus atmosphere characterization proposed in the Venus Life Finder Mission Study by Seager [59]. Seager explores how a comparatively small payload can be leveraged to gather significant data from Venus, with a special focus on looking for potential organic material. In addition, the Seager paper poses the Static Drop as a first step before more intensive exploration with balloons [59], which parallels our mission, even if the Seager plan calls for a high-altitude balloon with attached probes instead of a low-altitude balloon. While utilizing a different approach, the Seager study highlights how careful use of disposable probes can lead to valuable data collection.
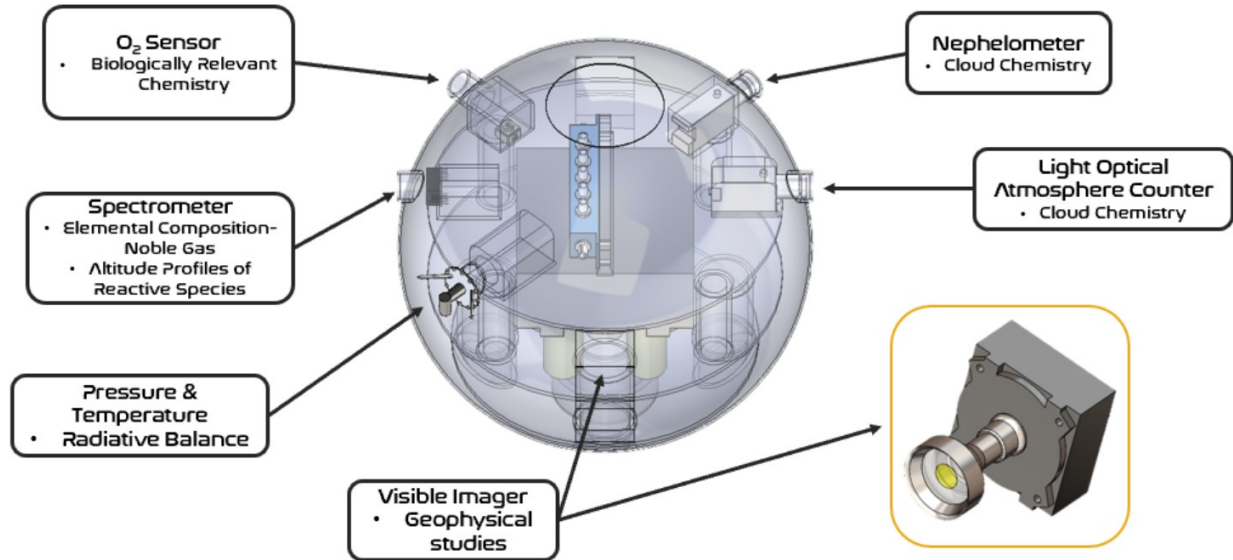
7.3 Static Drop Payloads

Figure 42: Payload Package within the static drop probe

For the static drop probe, to maximize scientific data return, there are eight instruments on each vehicle. As with most vehicles, an environmental suite is added to the system. In this case, this includes pressure and temperature sensors used for radiative balance, and an oxygen sensor meant to determine biologically relevant chemistry within the upper atmosphere.

The UV and IR spectrometers are used for determining the scattering properties of elements in the atmosphere that are sensitive to both infrared and ultraviolet light. During descent, the instruments can determine altitude profiles of reactive species and elemental composition of the noble gases.

Along with element configuration, cloud chemistry is measured by a nephelometer that measures the concentration of suspended particulates within the Venusian atmosphere and a light optical atmosphere counter that can determine the atmospheric composition and dynamics of the planet's atmosphere. A visible imager is the final instrument within the payload suite and is meant to conduct geophysical studies.

7.4 Static Drop Structures and Configurations

The Static Drop can essentially be divided into two parts: a small pressure vessel containing scientific instruments, and a larger heatshield and backshell that helps the Static Drop survive descent. The body of the outer container is composed of 3D-printed titanium that has an ablative carbon phenolic heat shield attached

to its bottom and RF transparent glass with an outer thermal protective layer of PTFE. The transparency of the glass allows for data collection during the descent, although all of said data collection is done by the internal probe. The probe on the inside is a pressure vessel to protect delicate parts like computers and previously described sensors, while also containing the batteries that keep the system running. Table 43 shows a more detailed diagram of the overall configuration of the static drop.
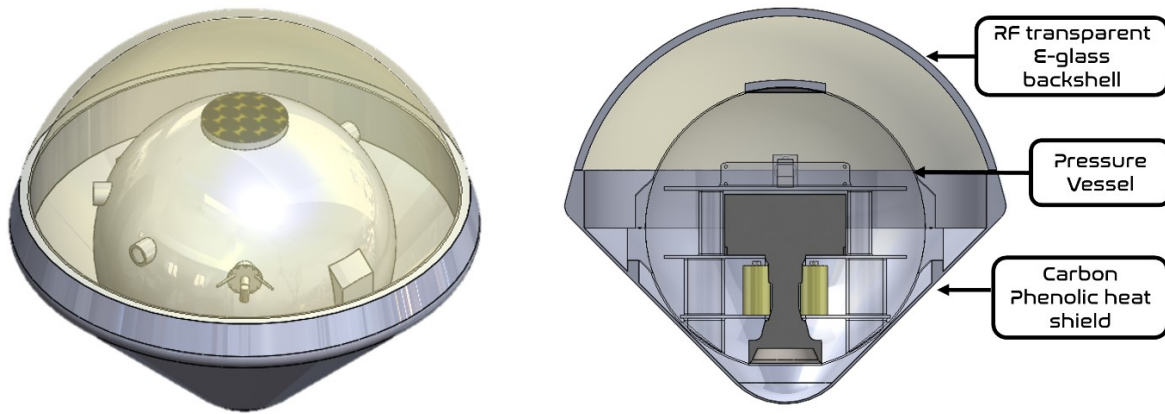

Figure 43: Overall configuration of the static drop probe

7.5 Static Drop Power

Based on extensive research about Venus' upper atmospheric conditions, the RHEIA^2 static drop probes will be powered using four primary batteries connected in parallel. The primary batteries will be lithium-thionyl chloride hybrid batteries. The power in the static drop will be controlled using a peak-power tracking technique with an unregulated bus.

The goal of the static drops is to deploy probes from the ITM down to Venus where it will conduct science return at the target altitude before it eventually reaches the surface and rapidly dissembles. Thus, when choosing a primary power source, solar arrays and radioisotope generators seemed inappropriate for the purpose of this system considering the system needed a power source that could be functional without a direct line of sight and can complete a less than 300-watt mission. Since the mission is concluded once the probe lands on the surface of Venus, a secondary, rechargeable battery is not necessary. The mission required a battery that could be stored for years at a time, have excellent specific energy, and last for hours within a wide range of temperatures; the lithium thionyl battery proved to be the only system that could accomplish all of these tasks.

Table 63: Li-SOCl$_2$ Battery performance

Specific Capacity (mAh/g)	Specific Energy (Wh/kg)	Volumetric Capacity (mAh/cm^3)
185	665	185

Table 64: Known values for Li-SOCl$_2$ battery performance

Operating Temperature ($^\circ C$)	Operating Pressure
-60 to 85	unknown

Table 65: Li-SOCl$_2$ battery specifications for use in the RHEIA^2 balloon system

Component	Mass (g)	Available Energy (W-hr)	Available Capacity (Ah)
Battery	92	61.2	17

Since many of these components have a fairly high TRL at the present, a 10% contingency and a margin of 30% to size the system appropriately. Table 66 breaks down the power required for the payload package during the three modes of the mission.

Table 66: Static Drop Package Power Budgets

Subsystem	Component	Descent			Science	
		Peak Power (W)	Duty Cycle (%)	Average Power (W)	Duty Cycle (%)	Average Power (W)
1 - Comms						
	1.1 X-band Transponder	26	10%	2.6	100%	26
	1.2 X-Band TWTA	50	10%	5	100%	50
	1.3 X-Band Antenna	5	10%	0.5	100%	5
2 - Payloads						
	2.1 - Nephelometer	5	0%	0	100%	5
	2.2 - Temperature Sensor	0	0%	0	100%	0
	2.3 - Pressure Sensor	1.5	0%	0	100%	1.5
	2.4 - Oxygen Sensor	0.45	0%	0	100%	0.45
	2.5 - UV Spectrometer	3.2	0%	0	100%	3.2
	2.6 - IR Spectrometer	0.3	0%	0	100%	0.3
	2.5 - Visible Imager	50	0%	0	100%	50
	2.6 - Light Optical Atmosphere Counter	20	0%	0	100%	20
3 - EDC						
	3.1 - IMU	12	100%	12	100%	12
4 - C&DH						
	4.1 - Processor	5	100%	5	100%	5
5 - Power						
	5.1 - PMAD/Wires	0.9	100%	0.9	100%	0.9
	Totals			35.75		245.6

Since it is estimated that it will take an estimated three hours for the static drop to be launched out of the ITM and enter Venus' atmosphere, the sizing and number of batteries to fulfill these time requirements have been calculated. Based on an estimated 257 Watts of total power available, Table 67 shows the battery lifetime estimates.

Table 67: Li-SOCl$_2$ Battery Lifetime Estimates

Power Mode	Lifetime Estimate (hours)
Launch	1.03
Descent	1.72
Science Return	1.24

7.6 Static Drop Thermal Control System

Because the static drop will be traveling from the ITM, through space, and into the Venusian atmosphere, thermal control is imperative to ensure the batteries, electronics, and payloads operate within a thermally regulated environment. To keep all the components within an optimal temperature range, a preliminary

thermal model utilized a static single-node model of the thermal environment of the static drop as seen in Fig. 44.
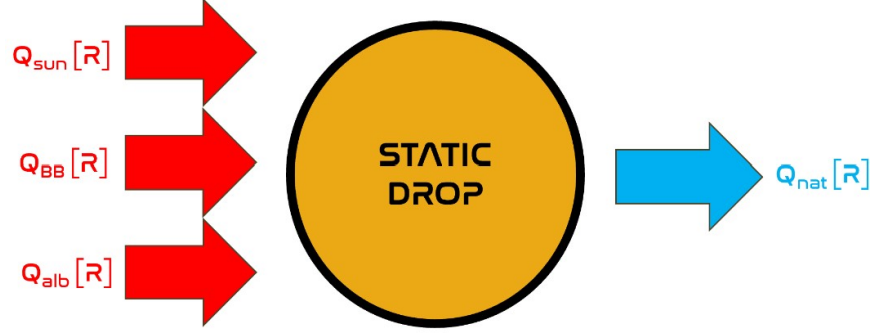

Figure 44: Static single node model representation of the static drop

After the initial node analysis, a mathematical examination is conducted. By calculating the overall effect of the thermal energy from the Sun, blackbody radiation, albedo, and the system's natural radiative energy, analysis of the worst-case thermal scenarios was conducted. As seen in Table 68, the hot and cold thermal analyses were calculated to find the expected thermal loads acting on the static drop.

Table 68: Static drop probe's thermal loads with no thermal control strategies.

	Earth	Venus
	Value (W)	Value (W)
Hot Case	258.0	460.7
Cold Case	2.61	-2.71

Overall, the thermal control strategies are designed to mitigate heat transfer from the harsh Venusian environment while regulating the temperature internally. Fig. 45 illustrates the two-node lumped parameter analysis conducted to access the internal and external thermal behaviors of the static drop. Thus, with an environment unfit for electronics, passive thermal control strategies prioritized by choosing Ti-6Al-4V shell for the probe along with a Silver Teflon coating. The titanium-alloy allows for high insulation and low thermal expansion of the system along with a coating that is highly resistant to damage from ultraviolet irradiation and solar winds. Since the system will experience drastically varied thermal environments from launch until landing, a lithium nitrate trihydrate phase-changing material is added to damp these thermal environment variations.
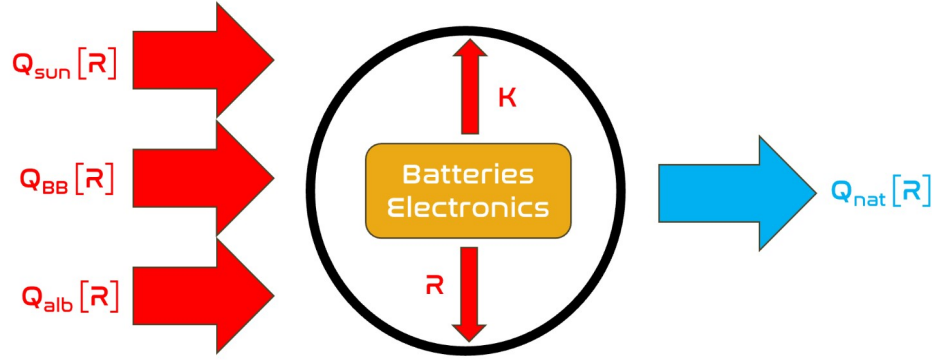
Figure 45: Thermal model representation of the static drop with two nodes: external and internal

7.7 Static Drop Communications

With six hours to complete a science return mission consisting of eight instruments, selecting an appropriate antenna to send information to the humans in the orbiter is crucial. Thus, an X-band patch antenna is attached the top of the static drop probe to downlink science and telemetry information from the the static drop to the orbiter. The antenna operates at 8025 MHz and requires a transmission power of 5 watts. The antenna has an area of 20 cm by 10 cm.

Because the static drops will be launched out of the ITM, it will be deployed and during landing on the surface, it will be a maximum of 500 km away from the system it is communicating with. Thus, lower frequency bands such as UHF or S-band prove to be insufficient, especially when considering the atmospheric losses experienced due to the thick Venusian clouds in the atmosphere. Table 69 provides the link budget for the system at maximum altitude.

Table 69: Link Budget for X-band antenna on Static Drop Probe

Link Budget: X-Band		
Transmitted Power	2	W
Transmitted Power	3.010	dB
Transmitted Power	33.01	dBm
Transmitter Antenna Gain	1.914	dB
Effective Antenna Gain	1.789	dB
Cable & Beam Loss	-4.9	dB
Path Loss	-104.5	dB
Atmospheric Loss	-0.02	dB
Receiver Power	-113.7	dBm
Receiver Antenna Gain	15.89	dB
CTR	76.30	dBhz
System Noise	-204.3	dBm/hz
Achieved Signal-to-Noise Ratio	14.28	dB
Required Signal-to-Noise Ratio	11	dB
Required Link Margin	**3.276**	

7.8 Static Drop Command and Data Handling

With just a two-hour science window to capture and record science data, having a sufficient command and data handling system that handles gathering, processing, and formatting data along with sending command signals and vehicle health records is crucial. For this system, a MIL-STD-1773 data bus is used since it is the most reliable and utilizes deterministic data transmission while also implementing multiple processing units for
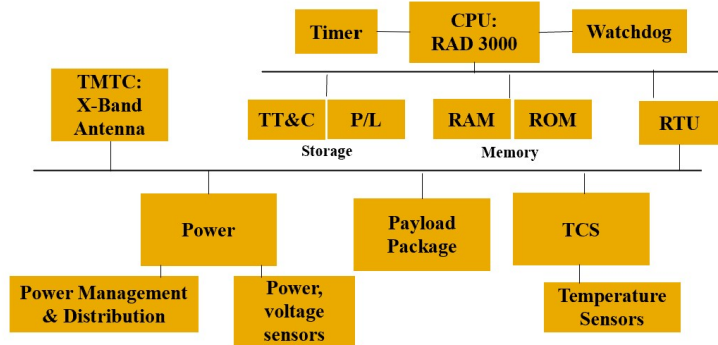

Figure 46: MIL-STD-1773 data bus architecture

increased performance. Illustrated in Fig. 46, this system allows for a data throughput up to 1 Mbps, requires 1 watt of power, and uses optical wires instead of electric so that it is both slightly more efficient and cost-effective compared to the usual MIL-STD-1553. Along with the data bus, a RAD 3000 CPU will be integrated into the system. With a 16 MB RAM and a maximum 10 MIPS sizing, this computer processing unit should be able to handle the processing of data throughout the mission, especially since the CPU is RAD hard which is ideal for the Venusian corrosive environment.
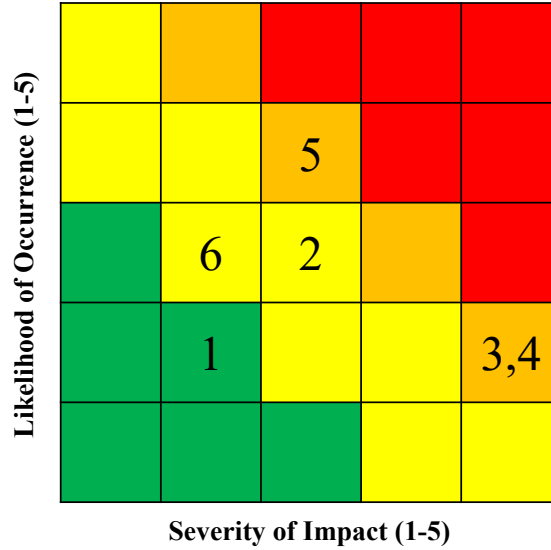
8 Risk Analysis

Figure 47: RHEIA^2 Risk Matrix

Table 70: RHEIA^2 Mission Risks

Risk Number	Vehicle/Subsystem	Title	Mitigation Strategy
R1	Chariot/EDL	Missing Landing Target	Implement reaction wheel control and further research potential issues with descent
R2	Chariot/Power	Unexpected high discharge rate	Ensure R&D focuses on test environment such as in GEER
R3	Chariot/Struct	Connection Failure	Conduct extensive hardware research into threading strategies
R4	ITM/ECLSS	Helium Leak	Include emergency air tanks for the astronauts in the ITM
R5	Static Drop/Prop & Chariot/Prop	SRB Ignition Failure	Conduct research to ensure SRBs fire within some specified time tolerance upon initiating descent
R6	Static Drop/Thermal	Early Instrument Failure	Use higher fidelity thermal analysis to determine if the science instruments are staying within their operating temperature

9 Mission Schedule and Cost

The total mission costs of RHEIA^2 were computed using NASA's Project Cost Estimating Capability (PCEC)[5]. This tool employs a robust cost model that outputs estimations based on a library of NASA cost estimating relationships for previous NASA missions. The PCEC template used was for a Near-Earth Robotic Spacecraft, which had Work Breakdown Structure (WBS) elements most similar to our mission. The Payloads under the WBS represent the Chariots and static probes aboard the ITM. The primary spacecraft in the WBS is the ITM. Added to the template's WBS was an ECLSS subsystem that is aboard the ITM to accurately reflect the ITM's costs. Otherwise, no other WBS elements were removed, added, or changed from the template. During the cost analysis, RHEIA^2 was specified as a directed, Class A planetary mission. Fig. 48 presents RHEIA^2's mission schedule by phase, which was specified when using the PCEC for cost estimations.
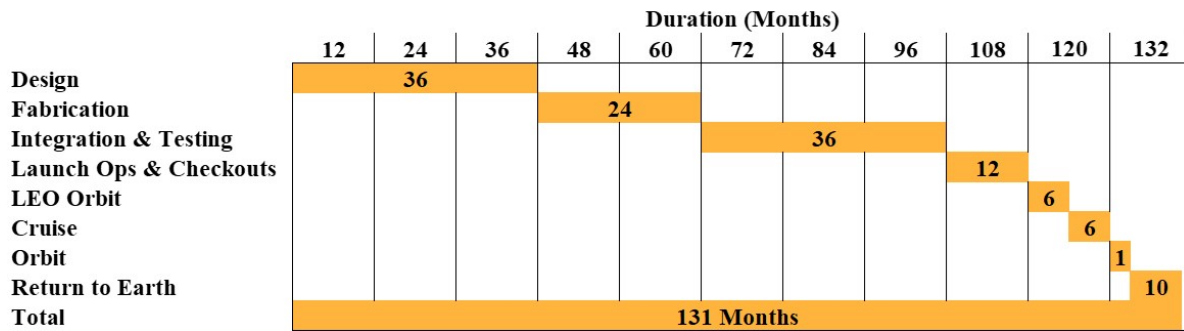

Figure 48: Gantt chart displaying the mission phase durations of RHEIA^2.

Sec. 9 exhibits RHEIA^2 complete cost estimation and WBS. The total cost, with 20% reserves reflecting a 20% mission cost margin, is $996.4 million (FY2023) with a 1.286 inflation factor[6] to convert FY2015 estimates to FY2023 estimates in the PCEC interface. This total mission cost meets the AIAA RFP mission budget requirement, stating that the "cost for the mission shall not exceed $1 Billion US Dollar (in FY23)." The low cost of the ITM displayed in Sec. 9 reflects the usage of COTS components and heritage subsystem design influences to reduce overall mission costs. To note, the cost analysis did not include any elements related to the human portion of the mission, consistent with the requirements in the RFP. Importantly, RHEIA^2's usage of a SpaceX launch vehicle and launch services would likely reduce the costs associated with the mission's Launch Vehicle/Services element in the WBS, which currently assumes more expensive traditional launch services and launch vehicle [60].

---

[5]https://www.nasa.gov/ocfo/pcec-project-cost-estimating-capability/
[6]https://data.bls.gov/cgi-bin/cpicalc.pl

WBS #	Level	Line Item Name/Description	Non-Recurring	Recurring Production	Non-Allocated	Operations	TOTAL
0	1	RHEIA[2]	$ 212.7	$ 416.4	$ 120.5	$ 80.7	$ 830.3
1.0	2	Project Management	$ 17.3	$ 25.6	$ -	$ -	$ 42.9
2.0	2	Systems Engineering	$ 5.0	$ 8.3	$ -	$ -	$ 13.3
3.0	2	Safety and Mission Assurance	$ 7.0	$ 19.1	$ -	$ -	$ 26.0
4.0	2	Science/Technology	$ -	$ -	$ 17.6	$ -	$ 17.6
5.0	2	Payloads: Chariots, Static Probes	$ 15.7	$ 28.3	$ -	$ -	$ 44.0
5.01	3	Payload Management	$ 4.1	$ 6.0	$ -	$ -	$ 10.0
5.02	3	Payload System Engineering	$ 1.0	$ 1.7	$ -	$ -	$ 2.8
5.03	3	Payload Product Assurance	$ 0.8	$ 2.1	$ -	$ -	$ 2.9
5.x	3	Payload I&T	$ 9.8	$ 18.5	$ -	$ -	$ 28.3
6.0	2	Flight System \ Spacecraft	$ 108.8	$ 196.7	$ -	$ -	$ 305.5
6.01	3	Flight System Project Management	$ 14.2	$ 20.9	$ -	$ -	$ 35.1
6.02	3	Flight System Systems Engineering	$ 3.5	$ 5.9	$ -	$ -	$ 9.4
6.03	3	Flight System Product Assurance	$ 5.7	$ 15.5	$ -	$ -	$ 21.2
6.10	3	Interplanetary Transfer Module (ITM)	$ 43.9	$ 75.9	$ -	$ -	$ 119.7
--	4	Structures & Mechanisms	$ 7.1	$ 24.6	$ -	$ -	$ 31.7
--	4	Thermal Control	$ 1.8	$ 5.8	$ -	$ -	$ 7.6
--	4	Electrical Power & Distribution	$ 5.0	$ 8.6	$ -	$ -	$ 13.6
--	4	GN&C	$ 0.6	$ 0.9	$ -	$ -	$ 1.4
--	4	Propulsion	$ 18.7	$ 22.7	$ -	$ -	$ 41.3
--	4	Communications	$ 4.4	$ 9.7	$ -	$ -	$ 14.1
--	4	ECLSS	$ 1.2	$ 1.5	$ -	$ -	$ 2.7
--	4	C&DH	$ 6.3	$ 3.6	$ -	$ -	$ 10.0
6.x	3	Flight System I&T	$ 41.6	$ 78.4	$ -	$ -	$ 120.0
7.0	2	Mission Operations System (MOS)	$ 16.9	$ 59.1	$ -	$ 80.7	$ 156.8
--	3	MOS/GDS Development (Phase B-D)	$ 16.9	$ 59.1	$ -	$ -	$ 76.0
--	3	Mission Ops & Data Analysis (Phase E)	$ -	$ -	$ -	$ 80.7	$ 80.7
8.0	2	Launch Vehicle/Services	$ -	$ -	$ 102.9	$ -	$ 102.9
9.0	2	System Integration, Assembly, Test & Check Out	$ 42.1	$ 79.2	$ -	$ -	$ 121.3

	Reserves %	w/Reserves
Reserves	20%	$ 996.4

10 Compliance Matrix

Table 71: RHEIA^2 Compliance Matrix

Topic	Included	Page Number	Note
Requirements	Yes	N/A	Requirements are listed alongside the discussion of the subsystems in their respective sections
CONOPS	Yes	11	
Trade Studies	Yes	Vehicles: 13 Subsystem: N/A	Subsystem trade studies are discussed alongside the discussion of the subsystems in their respective sections
Design Integration	Yes	ITM: 27 Chariot: 58 Static Drop: 77	
Cost Estimate	Yes	88	
Mission Operation and Summary	Yes	N/A	Summary tables are included in their relevant sections where applicable
Schedule	Yes	86	
Executive Summary	Yes	6	
References	Yes	94	

Acknowledgements

References

[1] Levin Gerdes et al. "Efficient autonomous navigation for planetary rovers with limited resources". In: *Journal of Field Robotics* 37.7 (2020), pp. 1153–1170. DOI: https://doi.org/10.1002/rob.21981. eprint: https://onlinelibrary.wiley.com/doi/pdf/10.1002/rob.21981.

[2] Philip G Neudeck Gary W Hunter Tibor Kremic. *High Temperature Electronics for Venus Surface Applications: A Summary of Recent Technical Advances.* Tech. rep. Glenn Research Center Cleveland, Ohio, United States: NASA, 2020. URL: https://ntrs.nasa.gov/citations/20205004681.

[3] AS Selivanov et al. "Evolution of the VENERA-13 imagery". In: *Soviet Astronomy Letters, vol. 8, July-Aug. 1982, p. 235, 236. Translation Pisma v Astronomicheskii Zhurnal, vol. 8, July 1982, p. 433-436* 8 (1982), p. 235.

[4] Geoffrey Landis. "Low-Altitude Exploration of the Venus Atmosphere by Balloon". In: *48th AIAA Aerospace Sciences Meeting Including the New Horizons Forum and Aerospace Exposition* (Jan. 2010). DOI: 10.2514/6.2010-628.

[5] John Connolly. *Deep Space Transport (DST) and Mars Mission Architecture.* NASA Mars Study Capability Team. [Online; accessed 24-April-2024]. Oct. 2017.

[6] Joseph A. Starek et al. "Fast, Safe, Propellant-Efficient Spacecraft Motion Planning Under Clohessy–Wiltshire–Hill Dynamics". In: *Journal of Guidance, Control, and Dynamics* 40.2 (2017), pp. 418–438. DOI: 10.2514/1.G001913.

[7] Chris D' Souza et al. "Orion Rendezvous, Proximity Operations and Docking Design and Analysis". In: *AIAA Guidance, Navigation and Control Conference and Exhibit*. DOI: `10.2514/6.2007-6683`. eprint: `https://arc.aiaa.org/doi/pdf/10.2514/6.2007-6683`. URL: `https://arc.aiaa.org/doi/abs/10.2514/6.2007-6683`.

[8] *Spacecraft Rendezvous and Docking - MATLAB & Simulink*. `https://www.mathworks.com/help/aeroblks/spacecraft-rendezvous-and-docking.html`.

[9] Koji Yamanaka et al. "Guidance and navigation system design of R-bar approach for rendezvous and docking". In: *17th AIAA International Communications Satellite Systems Conference and Exhibit*. DOI: `10.2514/6.1998-1299`. eprint: `https://arc.aiaa.org/doi/pdf/10.2514/6.1998-1299`. URL: `https://arc.aiaa.org/doi/abs/10.2514/6.1998-1299`.

[10] NASA. *NASA Trajectory Browser*. Accessed: 2024-04-25. 2024. URL: `https://trajbrowser.arc.nasa.gov/index.php`.

[11] NASA Jet Propulsion Laboratory. *NAIF Toolkit for MATLAB*. Accessed: 2024-04-25. 2024. URL: `https://naif.jpl.nasa.gov/pub/naif/toolkit_docs/MATLAB/index.html`.

[12] John C. Connolly. *Title of the Presentation [Replace with Actual Title]*. Accessed: 2024-04-25. 2024. URL: `https://nvite.jsc.nasa.gov/presentations/b2/D1_Mars_Connolly.pdf`.

[13] G. Pulci et al. *Carbon-phenolic abaltive materials for re-entry space vehicles: Manufacturing and properties*. Tech. rep. University of Rome, 2010.

[14] George P Sutton and Oscar Biblarz. *Rocket propulsion elements*. John Wiley & Sons, 2016.

[15] Malcolm A Fox. "Explosives and Class 1". In: *Glossary for the Worldwide Transportation of Dangerous Goods and Hazardous Materials*. Springer, 1999, pp. 74–85.

[16] Blue Canyon Technologies. *RW4 Reaction Wheels Datasheet*. 2024. URL: `https://storage.googleapis.com/blue-canyon-tech-news/1/2024/03/Reaction-Wheels-Large-Wheels-2024.pdf`.

[17] NASA. "NASA Spaceflight Human-System Standard Volume 2: Human Factors, Habitability, and Environmental Health". In: *NASA Technical Standard*. Vol. 2. 2023. URL: `https://standards.nasa.gov/sites/default/files/standards/NASA/D/nasa-std-3001-vol-2-rev-d-signature.pdf`.

[18] ESA. *European Columbus Laboratory]*. Accessed: 2024-04-25. URL: `https://www.esa.int/Science_Exploration/Human_and_Robotic_Exploration/Columbus/European_Columbus_laboratory`.

[19] JAXA. "Kibo Handbook". In: 2007. URL: `https://humans-in-space.jaxa.jp/library/item/kuoa/kuoa_kibo-handbook_en.pdf`.

[20]   NASA. *NASA Readies Commercial Air Tanks for Space]*. Accessed: 2024-04-25. URL: `https://www.nasa.gov/image-article/nasa-readies-commercial-air-tanks-space/`.

[21]   XS Scuba. *Luxfer Limited 106]*. Accessed: 2024-04-25. URL: `https://www.xsscuba.com/luxfer-limited-106-composite-cylinder`.

[22]   NASA. "Fire Protection". In: *NASA-STD-3001 Technical Brief*. 2023. URL: `https://www.nasa.gov/wp-content/uploads/2023/12/ochmo-tb-008-fire-protection.pdf`.

[23]   Afaf M Abd El-Hameed and YA Abdel-Aziz. "Aluminium alloys in space applications: a short report". In: *Journal of Advanced Research in Applied Sciences and Engineering Technology* 22.1 (2021), pp. 1–7.

[24]   Eberhard Schneider et al. "Advanced shields for manned space modules". In: *55th International Astronautical Congress of the International Astronautical Federation, the International Academy of Astronautics, and the International Institute of Space Law*. 2004, IAA–5.

[25]   JG Bakuckas, Steven R Thompson, and Richard C Rice. "Metallic Materials Properties Development and Standardization (MMPDS) Continuation and Replacement for MILHDBK-5". In: *Proceedings of the USAF Aircraft Structural Integrity Program (ASIP) 2002 Conference*. 2002.

[26]   Ram K Tripathi. *Meeting the Grand Challenge of Protecting Astronauts Health: Electrostatic Active Space Radiation Shielding for Deep Space Missions*. Tech. rep. 2016.

[27]   Eric L Christiansen et al. "Space station MMOD shielding". In: *Acta Astronautica* 65.7-8 (2009), pp. 921–929.

[28]   Ryan B Norman et al. "Early results from the advanced radiation protection thick GCR shielding project". In: *Applied Space Environments Conference (ASEC) 2017*. NF1676L-27179. 2017.

[29]   John F Lewis et al. "International space station (ISS) oxygen high pressure storage management". In: *SAE transactions* (2004), pp. 1399–1404.

[30]   Michael Kezirian, Kevin Johnson, and Stuart Phoenix. "Composite overwrapped pressure vessels (COPV): Flight rationale for the Space Shuttle Program". In: *AIAA SPACE 2011 Conference & Exposition*. 2011, p. 7363.

[31]   Harry W Jones. "Oxygen Storage Tanks Are Feasible for Mars Transit". In: *International Conference on Environmental Systems (ICES)*. ICES-2017-89. 2017.

[32]   Céline Cénac-Morthé et al. "Rosetta Lander batteries experience during all operation phases". In: *E3S Web of Conferences*. Vol. 16. EDP Sciences. 2017, p. 06006.

[33] Eric B Gietl et al. "The electric power system of the International Space Station-a platform for power technology development". In: *2000 IEEE Aerospace Conference. Proceedings (Cat. No. 00TH8484)*. Vol. 4. IEEE. 2000, pp. 47–54.

[34] Robert Scheidegger and James Soeder. "Spacecraft bus voltage selection". In: *Annual Space Power Workshop*. GRC-E-DAA-TN22245. 2015.

[35] Mihriban Whitmore, Jennifer Boyer, and Keith Holubec. "NASA-STD-3001, space flight human-system standard and the human integration design handbook". In: *Industrial and Systems Engineering Research Conference*. JSC-CN-25695. 2012.

[36] D.G. Gilmore. *Spacecraft Thermal Control Handbook Vol. 1: Fundamental Technologies*. The Aerospace Corporation, 2002.

[37] Isidoro Martinez. "Radiative view factors". In: *Universidad Politécnica de Madrid* (2015).

[38] James F Peter. "A Technical Overview of the Passive Thermal Control System for the Space Station Freedom". In: (1992).

[39] Patrick Oger et al. *ATV Thermal Control: Architecture and Jules Verne First Flight Results*. Tech. rep. SAE Technical Paper, 2009.

[40] J Tuttle et al. "THERMAL PROPERTIES OF DOUBLE-ALUMINIZED KAPTON AT LOW TEMPERATURES". In: *AIP conference Proceedings*. Vol. 986. 1. American Institute of Physics. 2008, pp. 34–41.

[41] RG Ross. "Quantifying MLI thermal conduction in cryogenic applications from experimental data". In: *IOP Conference Series: Materials Science and Engineering*. Vol. 101. 1. IOP Publishing. 2015, p. 012017.

[42] Stefano Rossi and Anton Ivanov. "Thermal model for cubesat: A simple and easy model from the Swisscube's thermal flight data". In: *Proceedings of the International Astronautical Congress*. Vol. 13. 2013, pp. 9919–9928.

[43] Lonny Kauder. *Spacecraft thermal control coatings references*. Tech. rep. 2005.

[44] Rubly, Robert P. and Taniguchi, Tetsuo. "Japanese Experiment Module Airlock Pressurization/Depressurization System Design and Development". In: *International Conference On Environmental Systems*. SAE International, June 1994. DOI: `https://doi.org/10.4271/941308`. URL: `https://doi.org/10.4271/941308`.

[45] Agilent. *IDP-10 Dry Scroll Pump]*. Accessed: 2024-04-25. URL: `https://www.agilent.com/en/product/vacuum-technologies/dry-scroll-pumps/idp-pumps/idp-10-dry-scroll-pump`.

[46] Hata, D., Brewer, E., and Louwagie, N. "An Introduction to Vacuum Systems". In: *Introduction to Vacuum Technology*. 2008. URL: https://milnepublishing.geneseo.edu/introtovacuumtech/front-matter/about-authors/.

[47] J.E. Blamont. "The VEGA Venus balloon experiment". In: *Advances in Space Research* (1987), pp. 295–298. ISSN: 0273-1177. DOI: 10.1016/0273-1177(87)90233-X.

[48] Anita Sengupta; Leslie Hall. *Challenges of a Venus entry mission*. Tech. rep. 2011.

[49] National Institute of Standards and Technology. *NIST Chemistry WebBook, SRD 69*. Accessed: 2024-05-02. URL: https://webbook.nist.gov/cgi/cbook.cgi?ID=C7732185&Mask=4&Type=ANTOINE&Plot=on.

[50] James Cutts et al. *Aerial Platforms for the Scientific Exploration of Venus Summary Report by the Venus Aerial Platforms Study Team*. Oct. 2018. DOI: 10.13140/RG.2.2.15808.89601.

[51] Siddharth Krishnamoorthy et al. "Progress Towards Balloon-Based Seismic Studies on Venus". In: *AGU Fall Meeting Abstracts*. Vol. 2022. Dec. 2022, P26B-05, P26B–05.

[52] Dean E. Glass et al. "High temperature primary battery for Venus surface missions". In: *Journal of Power Sources* 449 (2020), p. 227492. ISSN: 0378-7753. DOI: https://doi.org/10.1016/j.jpowsour.2019.227492.

[53] Eric Scherzberg and Thomas Miller. *Long Life Molten Salt Battery for NASA Venus Application*. Tech. rep. Glenn Research Center Cleveland and Advanced Thermal Batteries, Inc., 2023.

[54] Geoffrey Landis and Emily Haag. "Analysis of Solar Cell Efficiency for Venus Atmosphere and Surface Missions". In: July 2013. DOI: 10.2514/6.2013-4028.

[55] Bong-Chull Kim et al. "All solid state Li-ion secondary battery with FeS anode". In: *Solid State Ionics* 176.31 (2005). 30th Symposium on Solid State Ionics in Japan, pp. 2383–2387. ISSN: 0167-2738. DOI: https://doi.org/10.1016/j.ssi.2005.05.019.

[56] David G. Gilmore. *Spacecraft Thermal Control Handbook*. Volume 1 - Fundamental Technologies (2nd Edition). American Institute of Aeronautics and Astronautics/Aerospace Press (AIAA), 2002. ISBN: 9780198520115.

[57] Judth C. Gomez. *High-Temperature Phase Change Materials (PCM) Candidates for Thermal Energy Storage (TES) Applications*. Tech. rep. National Renewable Energy Laboratory, 2011.

[58] J. Hoffman H. L. Justh A. M. Dwyer Cianciolo. *Venus Global Reference Atmospheric Model (Venus-GRAM): User Guide*. Tech. rep. National Aeronautics and Space Administration, 2021.

[59]   Sara Seager et al. *Venus Life Finder Mission Study*. 2021. arXiv: `2112.05153 [astro-ph.IM]`.

[60]   Harry Jones. "The recent large reduction in space launch cost". In: 48th International Conference on Environmental Systems. 2018.